Nerve growth factor stimulates axon outgrowth through negative regulation of growth cone actomyosin restraint of microtubule advance

Stephen G. Turney[a], Mostafa Ahmed[b,*], Indra Chandrasekar[b,†], Robert B. Wysolmerski[c], Zoe M. Goeckeler[c], Robert M. Rioux[d,‡], George M. Whitesides[d], and Paul C. Bridgman[b]
[a]Center for Brain Science and Department of Molecular and Cellular Biology and [d]Department of Chemistry and Chemical Biology, Harvard University, Cambridge, MA 02138; [b]Department of Neuroscience, Washington University School of Medicine, St. Louis, MO 63110; [c]Department of Neurobiology and Anatomy, West Virginia University School of Medicine, Morgantown, WV 26506

ABSTRACT **Nerve growth factor (NGF) promotes growth, differentiation, and survival of sensory neurons in the mammalian nervous system. Little is known about how NGF elicits faster axon outgrowth or how growth cones integrate and transform signal input to motor output. Using cultured mouse dorsal root ganglion neurons, we found that myosin II (MII) is required for NGF to stimulate faster axon outgrowth. From experiments inducing loss or gain of function of MII, specific MII isoforms, and vinculin-dependent adhesion-cytoskeletal coupling, we determined that NGF causes decreased vinculin-dependent actomyosin restraint of microtubule advance. Inhibition of MII blocked NGF stimulation, indicating the central role of restraint in directed outgrowth. The restraint consists of myosin IIB- and IIA-dependent processes: retrograde actin network flow and transverse actin bundling, respectively. The processes differentially contribute on laminin-1 and fibronectin due to selective actin tethering to adhesions. On laminin-1, NGF induced greater vinculin-dependent adhesion–cytoskeletal coupling, which slowed retrograde actin network flow (i.e., it regulated the molecular clutch). On fibronectin, NGF caused inactivation of myosin IIA, which negatively regulated actin bundling. On both substrates, the result was the same: NGF-induced weakening of MII-dependent restraint led to dynamic microtubules entering the actin-rich periphery more frequently, giving rise to faster elongation.**

Monitoring Editor
Paul Forscher
Yale University

Received: Sep 8, 2015
Revised: Nov 23, 2015
Accepted: Nov 24, 2015

This article was published online ahead of print in MBoC in Press (http://www.molbiolcell.org/cgi/doi/10.1091/mbc.E15-09-0636) December 2, 2015.

Present addresses: *Brooke Army Medical Center, Ft. Sam Houston, TX 78234; †Sanford Children's Health Research Center, Sanford Research, Sioux Falls, SD 57104; ‡Department of Chemical Engineering, Pennsylvania State University, University Park, PA 16802.

Address correspondence to: Paul C. Bridgman (bridgmap@pcg.wustl.edu).

Abbreviations used: Bleb, blebbistatin; C3, exoenzyme C3 transferase; CCD, charge-coupled device; CT, control; DRG, dorsal root ganglion; EB3, dynamic microtubule plus end–binding family protein; FN, fibronectin; GFP, green fluorescent protein; LE, leading edge; LED, light-emitting diode; LN, laminin-1; MII, nonmuscle myosin II; MIIA, nonmuscle myosin IIA; MIIB, nonmuscle myosin IIB; MIIB KO, nonmuscle myosin IIB knockout; MIIC, nonmuscle myosin IIC; MLC, myosin light chain; NGF, nerve growth factor; NT-3, neurotrophin-3; PEI, polyethylenimine; PL, polylysine; PLO, poly-L-ornithine; pMLC, phosphorylated myosin light chain; shRNAi, short hairpin RNA interference; tdEOS, tandem dimer EosFP; Tyr Tub, tyronsinated tubulin; Wt, wild type.

INTRODUCTION

Trophic signaling is essential to the self-organizing behavior of neurons (Harrington and Ginty, 2013). In particular, many neurons require interaction with trophic factors to survive during development. These factors may be available only close to target and support cells; therefore survival can depend on the level of secretion and the ability of neurons to extend axons that reach the sources of secretion. For example, sensory axons that innervate skin are known to first grow in response to NT-3 (Coggeshall *et al.*, 1994; Gaese *et al.*, 1994). They become nerve growth factor (NGF) dependent near the target tissue, likely because NGF is released as a diffusible factor and is present at lower concentrations far from the target tissue. The axons grow into the target tissue (i.e., toward a higher concentration of NGF), where they arborize and terminate (Albers and Davis, 2007). Thus neuron survival depends on the level of NGF secretion in the target tissue and the fact that NGF directly stimulates and guides axon growth (Gundersen and Barrett, 1980; Gallo *et al.*, 1997). The mechanisms by which NGF promotes neuronal cell

Supplemental Material can be found at:
http://www.molbiolcell.org/content/suppl/2015/11/29/mbc.E15-09-0636v1.DC1.html

survival have been studied extensively (Oppenheim, 1989; Huang and Reichardt, 2001; Ichim *et al.*, 2012). It is unclear, however, how NGF signaling influences the speed and direction of axon growth.

Previous studies have shown that axon growth occurs as a consequence of growth cone advance and that, like a cell body, the growth cone integrates input signals and then executes specific behaviors in response (Goldberg and Burmeister, 1986; Wen and Zheng, 2006; Lowery and Van Vactor, 2009). The molecular clutch hypothesis provides a framework for understanding how the growth cone executes forward advance (Mitchison and Kirschner, 1988). In leading-edge protrusions, actin filaments are continually assembled and disassembled at the distal and proximal ends, respectively, giving rise to retrograde actin flow (Lin and Forscher, 1995; Lin *et al.*, 1996; Burnette *et al.*, 2008). Myosin II (MII) contributes to the strength and speed of retrograde actin flow through its effects on bundling and rearward pulling of an actin filament network. Retrograde actin flow efficiently sweeps back dynamic microtubules (Schaefer *et al.*, 2002; Rodriguez *et al.*, 2003; Schaefer *et al.*, 2008). Cytoskeletal coupling at focal adhesion sites (the molecular clutch) can cause slowing of retrograde actin flow, making it likelier that microtubules invade the periphery (Suter *et al.*, 1998, 2004; Robles and Gomez, 2006; Lee and Suter, 2008). The cortex consolidates around microtubules, stimulating further protrusive activity and concomitant axon extension (Mitchison and Kirschner, 1988; Burnette *et al.*, 2008).

It remains unclear how NGF influences this process. Prior work implicated direct regulation of microtubule dynamics, actin dynamics, and local protein synthesis (Tanaka and Kirschner, 1991; Goold and Gordon-Weeks, 2003; Gehler *et al.*, 2004; Zhou *et al.*, 2004; Hengst *et al.*, 2009). Does one effect or another have a predominant role? Two findings suggest the actin cytoskeleton is the primary regulatory control point. First, NGF stimulates faster axon growth in both embryonic and adult sensory neurons on laminin-1 (LN) or fibronectin (FN) but not on synthetic polypeptides such as polylysine or polyornithine, and thus it may regulate cytoskeletal coupling (Liu *et al.*, 2002; Tucker *et al.*, 2006). Second, MII activity is required for fast sensory axon growth on LN (Turney and Bridgman, 2005; Ketschek *et al.*, 2007). Thus we hypothesized that NGF has local direct effects on actin cytoskeletal processes that influence axon growth rates. To test this possibility, we assessed whether NGF stimulation is MII dependent.

For this work, we grew embryonic mouse dorsal root ganglion (DRG) explants or dissociated cells in different concentrations of NGF on coverslips coated with LN or FN to compare the growth-promoting effect of NGF on different stimulation-supporting substrates. Using genetic and biochemical techniques, we induced gain or loss of function to test the role of myosin II isoforms, RhoA, and vinculin. From fixed-time-point and time-lapse imaging, we assessed axonal outgrowth rates and the organization or dynamics of fluorescently labeled growth cone cytoskeletal components.

RESULTS

Stimulation of axon elongation on LN by NGF requires MII activity

Previous work showed that peripheral axon elongation on LN is slower after inhibition of MII activity (Turney and Bridgman, 2005; Ketschek *et al.*, 2007) and for neurons harvested from MIIB-knockout mice versus controls (Tullio *et al.*, 2001). In these studies, the neurons were cultured in growth medium containing NGF. However, NGF was used at a fixed concentration, and thus the contribution of NGF to MII-dependent faster outgrowth was not tested. Does NGF stimulation require MII activity? To answer this question, we first confirmed that NGF stimulation is substrate dependent. Increasing the concentration of NGF from 0.5 (low) to 50 ng/ml (high) stimulated axon outgrowth as expected for embryonic mouse DRG explants on LN (Figure 1, A and B; *t* test, $p < 0.005$) but not on the synthetic polypeptides poly-L-ornithine (PLO) and polyethylenimine (PEI; PLO, high NGF rate, 7.6 ± 0.4 µm/h; low NGF rate, 6.4 ± 0.5 µm/h; *t* test, $p > 0.1$; PEI, high NGF rate, 7.8 ± 0.4 µm/h; low NGF rate, 7 ± 0.5 µm/h; *t* test, $p > 0.1$). Thus, if MII supports NGF stimulation of axon outgrowth, it does so on LN but not on PLO or PEI.

To determine whether MII activity is required for NGF stimulation, we varied the concentration of NGF and chronically treated explants on LN with blebbistatin, a MII-specific inhibitor. Under this condition, axon outgrowth was the same in both low and high NGF; this rate was slow compared with untreated control cells in high NGF (Figure 1B). Thus inhibition of MII completely blocked NGF-mediated stimulation of faster elongation on LN and caused overall slowing of axon outgrowth (analysis of variance [ANOVA], $p < 0.0001$). The slowing appears to depend strongly on the substrate formulation. We found that maximal outgrowth rates (~25 µm/h) were obtained on substrates that were created using high concentrations of LN (20 µg/ml) plus polyornithine (100 µg/ml). Outgrowth rate is slower (7–11 µm/h) and has the opposite response to MII inhibition on substrates produced using low concentrations of LN (5–10 µg/ml) plus polylysine (PL; 100 µg/ml; Hur *et al.*, 2011), PL (100 µg/ml), or PLO (100 µg/ml; Turney and Bridgman, 2005; Ketschek *et al.*, 2007). To verify that an opposite response is produced with mouse DRG neurons, we chronically treated cells growing on PLO (100 µg/ml) with blebbistatin (Bleb). The outgrowth rate increased compared with controls (see prior discussion), and this was independent of the concentration of NGF (PLO, high NGF + Bleb, rate = 13.5 ± 0.4 µm/h; low NGF + Bleb, rate = 13.1± 0.5 µm/h; *t* test, $p \geq 0.54$, n.s.).

NGF stimulation of faster axon outgrowth on fibronectin requires MII activity but involves a different regulatory pathway

The rate of axon elongation on FN is responsive to NGF-mediated stimulation, albeit to a lesser degree than on LN (Figure 1C; *t* test, $^{**}p < 0.001$). Therefore we tested whether faster elongation in response to NGF on FN is MII dependent. As observed on LN, chronic treatment with the MII inhibitor blebbistatin produced the same rate of outgrowth in low and high NGF, eliminating the stimulatory effect (Figure 1C; ANOVA, $^{*}p < 0.0001$). Thus MII activity is required for NGF stimulation on both substrates and is therefore likely to be required for all substrates that support stimulation; however, in contrast to what was observed on LN, chronic blebbistatin treatment did not slow the overall rate of elongation observed in high NGF. It significantly increased the rate of outgrowth compared with the rate observed in low NGF, indicating that in this condition, MII negatively regulates or restrains outgrowth on FN (Figure 1C). In this regard, FN was similar to PL or PLO; outgrowth rates on FN were significantly slower than on LN (20 µg/ml), and inhibition of MII caused an increase in the rate. However, unlike PL or PLO, FN substrates supported NGF stimulation, which eliminated the differences between high NGF and MII inhibition.

RhoA inhibition produces substrate-dependent effects on axon elongation

Binding of NGF to p75NTR, the low-affinity NGF receptor, promote fasters elongation of ciliary axons by direct inactivation of RhoA (Yamashita *et al.*, 1999). RhoA-dependent pathways also regulate MII activity in axonal growth cones (Loudon *et al.*, 2006) and specifically

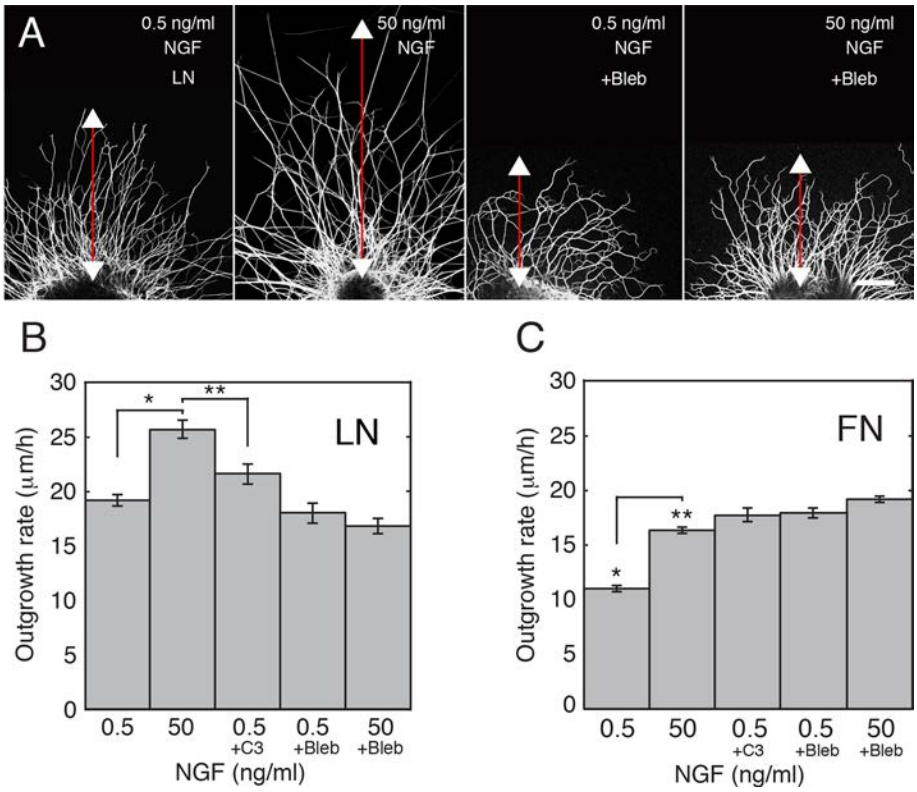

FIGURE 1: Stimulation of faster DRG axon elongation on LN by NGF is MII dependent. (A) Examples of explants on LN fixed 20 h after plating and stained for neurofilaments. Explants were imaged by confocal microscopy. The length of outgrowth was measured to determine the effects of NGF and chronic application of blebbistatin (50 μM, applied 2 h after plating). Application of the inactive (+) form of blebbistatin had no detectable effect on outgrowth (not shown). Bar, 100 μm. (B) High NGF (50 ng/ml) induces a significant increase in axon outgrowth rate on LN. Treatment with C3 (2 μg/ml overnight) causes an increase in elongation rate but less than that induced by high NGF. Treatment with blebbistatin causes a decrease in elongation rate and also blocks the stimulative effect of NGF. Differences were significant by ANOVA ($p < 0.0001$) and retrospective *t* tests (*$p < 0.005$, **$p < 0.05$). $N = 54$, 37, 27, 45, and 51 explants per category, respectively (from five experiments). (C) NGF stimulation of faster DRG axon elongation on FN is also MII dependent. Axon elongation from DRG explants grown overnight on FN is significantly faster in high NGF than in low NGF. RhoA inhibition using C3 transferase (C3; 2 μg/ml, overnight) or MII inactivation using blebbistatin applied 2 h after plating causes a significant increase in elongation rates independent of the level of NGF; ANOVA ($P < 0.0001$) and retrospective *t* test (**$p < 0.001$). $N = 12$, 13, 8, 19, and 12 explants per category, respectively (from three experiments).

have effects on transverse actin "arcs" (Zhang *et al.*, 2003) and filopodia (Gehler *et al.*, 2004). To determine whether inhibition of RhoA activity mimics the stimulative effect of NGF, we treated DRG neurons on LN growing in low NGF with C3 transferase (2 μg/ml), a cell-permeable pharmacologic RhoA inhibitor. The rate of axon elongation increased but was significantly lower than that obtained with high NGF (Figure 1B; *t* test, $p < 0.05$). In contrast, inhibition of RhoA with C3 transferase (same dose) in DRG neurons growing on FN had nearly the same effect as NGF in stimulating faster outgrowth (Figure 1C). Thus a single dose of C3 transferase can mimic the effect of NGF or MII inhibition on outgrowth rates observed on FN but not on LN.

NGF reduces myosin light chain phosphorylation (MII activity) on FN but not on LN

The fact that MII activity is required for faster outgrowth in response to NGF but appears to have complementary roles on LN and FN raises the possibility that the individual MII isoforms are differentially regulated. To test whether NGF directly regulates MII isoform activity, we assessed growth cone myosin light-chain (MLC) phosphorylation using fluorescence ratio imaging. First we labeled growth cones with a polyclonal antibody that recognizes phosphorylated MLC (Ser-19) and a monoclonal antibody against total MLC. High NGF significantly decreased MLC phosphorylation on FN (Figure 2A; ANOVA, *$p < 0.001$) but not on LN (ratio pMLC/MLC for 50 ng/ml NGF, 4.8 ± 0.3; for 0.5 ng/ml NGF, 4.5 ± 0.3; *t* test, $p = 0.5$). Treatment with RhoA inhibitor C3 transferase had a similar effect (Figure 2A). DRG neurons express all three isoforms of nonmuscle MII (Figure 2, A–C; Brown *et al.*, 2009). To determine whether the decrease in total MLC phosphorylation is due to inactivation of a specific isoform of MII, we overexpressed different green fluorescent protein (GFP)–MII isoforms and correlated the fluorescence intensity of GFP with that of the phosphorylation-specific antibody in growth cones (Figure 2, B and C). An increase in NGF concentration produced a large decrease in the phosphorylation of the MLC associated with GFP-MIIA in growth cones on FN (Figure 2B). The change in phosphorylation of the MLC associated with GFP-MIIB was comparatively small (Figure 2C). No significant changes for any of the isoforms were detected for growth cones on LN. These results indicate that on FN, NGF significantly reduces the activity of MIIA but not that of MIIB (or IIC). The effect is detectable only on FN, suggesting that NGF may regulate faster growth through more than one MII-dependent mechanism.

MIIB knockout slows outgrowth and eliminates the growth-promoting role of MII on LN

To determine whether negative regulation of MIIA (or IIC) was sufficient for the MII-dependent stimulation of axon outgrowth, we grew DRG neurons from MIIB knockout (KO) mice on LN and FN. The stimulatory effect of NGF was significant but diminished in the MIIB KO cells on LN compared with controls (CT; Figure 3A; *t* tests , *$p < 0.005$, **$p < 0.05$), and the outgrowth rates were slower in both low and high NGF. The slower outgrowth rate in high NGF was partially reversed by treatment with blebbistatin, indicating that MIIA contributes to a restraining effect on LN even in the presence of high NGF concentration (Figure 3B; *t* test, $p < 0.05$). The absence of a slowing effect in response to blebbistatin treatment indicates that MIIB is responsible for the growth-promoting effect of NGF on LN, as we previously proposed (Turney and Bridgman, 2005). However the restraining effect of MIIA on LN was smaller than that observed for CT cells on FN (Figure 2A), suggesting that NGF directly regulates MIIA activity on LN but to a lesser degree than on FN. In contrast to the results on LN, NGF stimulated an increase in outgrowth rate on FN that was the same for both MIIB KO cells and CT cells (Figure 3C; *t* tests, both *$p < 0.001$), consistent with the idea that NGF primarily regulates MIIA activity on FN.

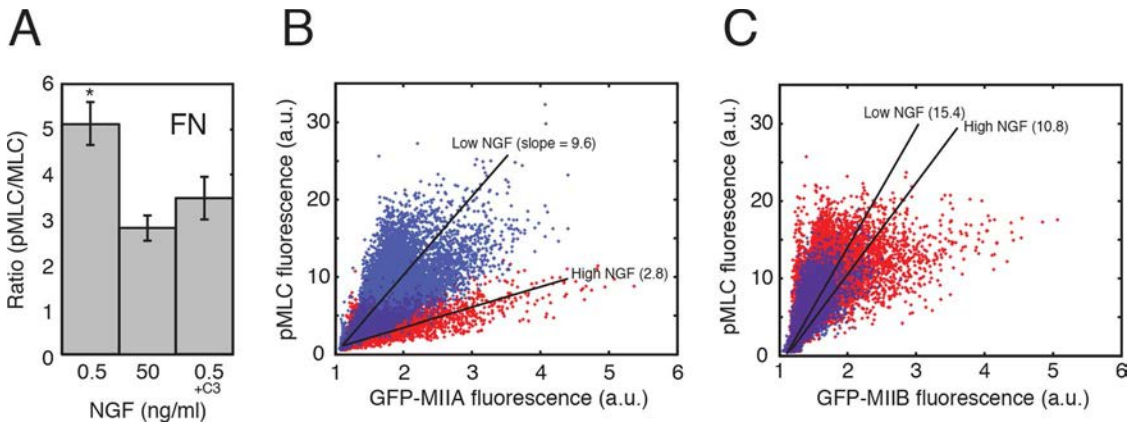

FIGURE 2: NGF reduces MIIA activity on FN. (A) MLC phosphorylation is significantly reduced in growth cones on FN in response to high NGF or treatment with C3 (ANOVA, $*p < 0.001$). $N = 12$ each. Values were determined using fluorescence ratio imaging (see *Materials and Methods*). No significant change was detected for growth cones on LN (unpublished data). (B, C) Representative scatterplots of fluorescently labeled pMLC vs different GFP-tagged MII heavy chain isoforms (GFP-tagged MIIC is not shown, but was similar to GFP-MIIB). (B) GFP-tagged MIIA and (C) GFP-tagged MIIB in low NGF (blue) and high NGF (red) for growth cones on FN. The GFP-tagged MII isoforms were highly overexpressed; therefore the pMLC signal was correlated with the expression level (and activity) of the GFP-tagged MII isoform. The intensity data are plotted pixel by pixel because of spatial variation in the distribution of MII within growth cones. High NGF caused a decrease in the pMLC signal for cells overexpressing MIIA. No effect was seen for cells overexpressing MIIB. (Using linear regression, the difference between the slopes for the sets of red and blue points is an order of magnitude greater for cells overexpressing MIIA than for cells overexpressing MIIB.) Thus NGF appears to directly regulate MIIA activity but not MIIB activity on FN. No changes were observed on LN (unpublished data). At least 10 growth cones were analyzed for each substrate (LN and FN) and level of NGF (low and high).

Furthermore, the outgrowth rates were proportionally higher for MIIB KO cells than for CT cells, suggesting that MIIB contributes somewhat to the slowing of advance (restraint) on FN, but its role appears to be unregulated by NGF. MIIB KO cells formed normal-appearing, vinculin-positive adhesion complexes and MIIA-positive bundles that varied with NGF concentration (Figure 3, D and F). Blebbistatin treatment appeared to alter the size and distribution of the vinculin-positive adhesion complexes; vinculin staining appeared only as spots (never elongated) and was eliminated from the leading edge (Figure 3, E and F). Transverse bundles were also eliminated, suggesting that MII-driven retrograde flow or traction may be required for bundle and adhesion complex formation and/or turnover (Figure 3, E and F).

MIIA knockdown increases elongation rates on FN

To determine whether changes in MIIA activity are required for the stimulatory effect of NGF on FN, we used short hairpin RNA interference (shRNAi) to knock down MIIA expression. In low NGF, partial knockdown of MIIA expression resulted in cells having longer neurites than did controls (Figure 4, A, B, and D; *t* test, $*p < 0.02$). Thus the knockdown of MIIA expression mimicked the stimulatory effect of NGF or MII inhibition with blebbistatin. It was difficult to assess the effect of knockdown on actin bundle organization quantitatively because growth cones were considerably attenuated in the 96-h cultures. However, in general, transverse bundles were only very rarely observed after knockdown. Similar experiments performed on LN did not produce a significant increase in outgrowth, probably because the knockdown was only partial, and MIIA activity contributes less to restraint on LN. These results are consistent with the idea that NGF stimulates faster neurite elongation on FN primarily by reducing MIIA activity.

NGF decreases retrograde flow rates on LN

The foregoing results indicate that MII plays a role in regulating NGF-stimulated axon elongation. Previous work has shown the following: 1) MII is important for driving retrograde flow of actin (Medeiros *et al.*, 2006), 2) retrograde flow opposes the advance of dynamic microtubules into the periphery of growth cones (Rodriguez *et al.*, 2003; Suter *et al.*, 2004; Schaefer *et al.*, 2008), 3) the rate of retrograde flow is inversely proportional to the rate of advance (Lin and Forscher, 1995), and 4) dynamic microtubules are important for growth cone advance and turning (Rochlin *et al.*, 1996; Challacombe *et al.*, 1997; Buck and Zheng, 2002). Does NGF regulate MII-driven retrograde flow of actin and thereby influence the probability of dynamic microtubule advance? To answer this question, we monitored retrograde flow and microtubule dynamics in neurons transfected with constructs for tdEOS-actin, GFP-LifeAct, or Ruby-LifeAct (to label actin) and GFP-EB3 or tdTomato-EB3 (to label dynamic microtubule plus ends), respectively (Stepanova *et al.*, 2003; Fischer *et al.*, 2006; Riedl *et al.*, 2008).

Retrograde flow was measured by tracking individual bright spots in time-lapse images of cells expressing tdEOS-actin (without photoconversion; Figure 5A) and doing kymograph analysis of GFP- or Ruby-LifeAct (Figure 5B). It was not possible to do fluorescent speckle analysis because speckle lifetimes were too short (<3 s). Spot-tracking measurements of tdEOS-actin revealed that the rate of retrograde flow in growth cones on LN was inversely related to the level of NGF (Figure 5C; *t* test, $p < 0.001$). A similar result was obtained from the kymograph analysis of fluorescent LifeAct (Figure 5D; *t* test, $p < 0.002$). However, the rates we measured were twofold higher for LifeAct than for tdEOS-actin. A difference between GFP-actin and GFP-LifeAct in measurements of retrograde flow has been reported previously (Riedl *et al.*, 2008). The rate of retrograde flow observed in unlabeled cells is close to that measured with LifeAct; therefore we used LifeAct for most experiments. Kymograph analysis showed that retrograde flow rates were high when growth cones were in low NGF on LN or FN (Figure 5, D and E). An increase in the level of NGF caused retrograde flow to slow down on LN but not on FN (*t* test, $p > 0.2$). These results support the idea that NGF works through different substrate-dependent mechanisms to stimulate

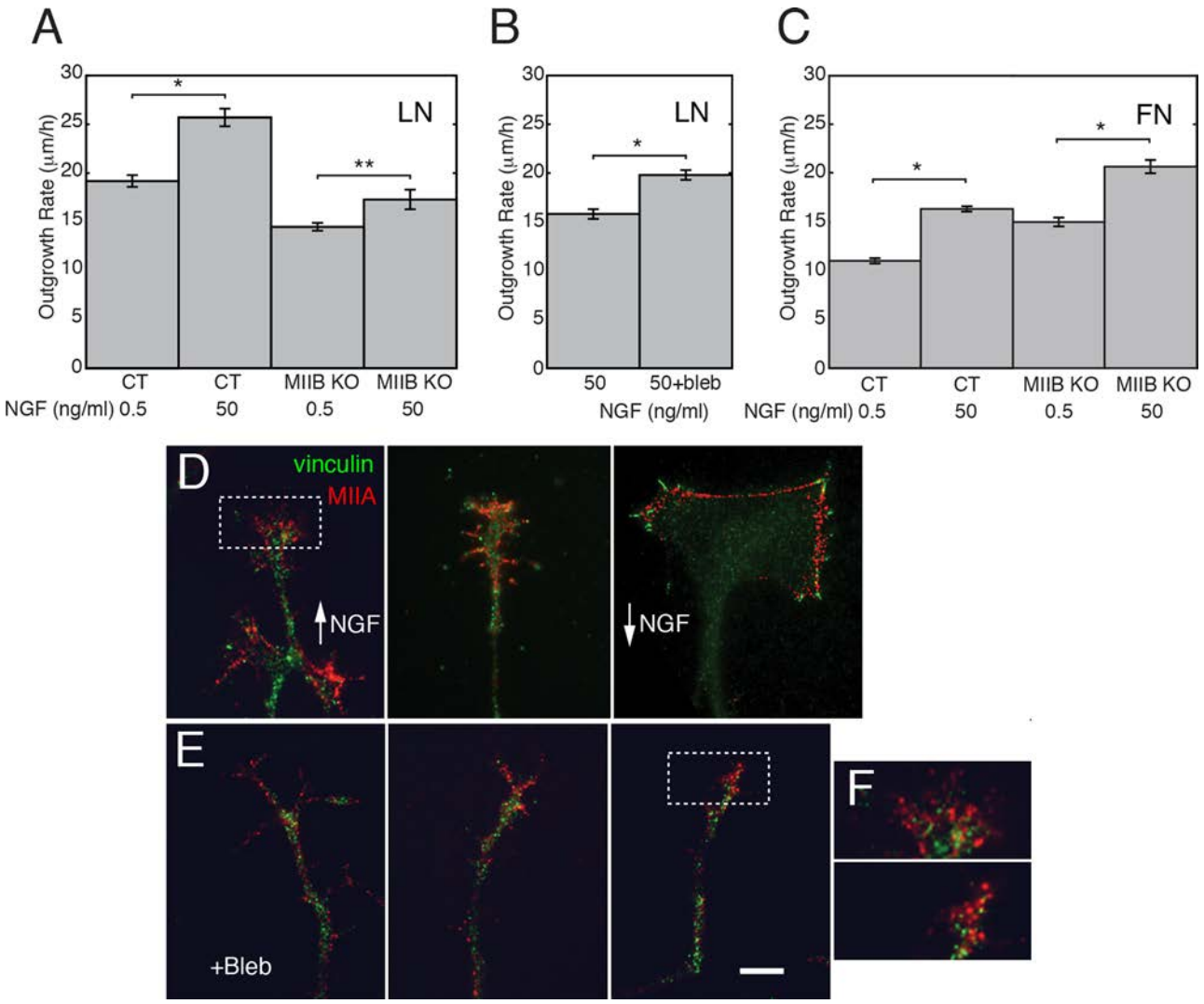

FIGURE 3: Negative regulation of MIIA activity by NGF contributes to the stimulatory effect on LN. (A) Comparison of the change in outgrowth rate resulting from NGF stimulation of control and MIIB KO neurons on LN. Axon outgrowth is generally slower for MIIB KO neurons than for controls (Tullio *et al.*, 2001). In addition, NGF has a smaller stimulative effect on MIIB KO cells than on control (CT; *t* tests, $*p < 0.005$, $**p < 0.05$). $N = 54$, 37, 22, and 56 explants respectively (from three experiments). (B) Blebbistatin treatment increases the outgrowth rate of MIIB KO neurons on LN, indicating that MIIA (IIC) has a restraining effect even in high NGF (*t* test, $*p < 0.05$). $N = 40$ and 41 explants (from three experiments). (C) NGF stimulates a significant increase (to the same degree as in control) in the rate of elongation of DRG neurons cultured from MIIB KO mice on FN (*t* test; $*p < 0.001$). $N = 8$ and 10 explants (from two experiments). In addition, the elongation rates on FN are proportionally higher for MIIB KO cells than for CT cells. Error bars indicate SEM. (D) Examples of MIIA and vinculin staining in growth cones of MIIB KO cells. Left and middle, staining for MIIA (red) and vinculin (green) in high NGF. Right, staining for MIIA and vinculin in low NGF. (E) Staining for MIIA and vinculin after treatment with blebbistatin. Vinculin spots are smaller, and MIIA bundles are eliminated. Bar, 10 μm. (F) Enlargements of the boxed regions in D and E.

axon elongation. NGF did not cause a detectable change in CT growth cone MII activity on LN (see foregoing results). Thus the decrease in retrograde flow rate is unlikely to be due to direct regulation of MII activity on LN.

NGF-mediated stimulation of outgrowth on LN correlates with increased adhesion–cytoskeletal coupling

A possible mechanism suggested by previous studies is that the decreased retrograde flow rates associated with faster growth are due to increased adhesion–cytoskeletal coupling (Lin and Forscher, 1995; Jurado *et al.*, 2005). To test whether NGF acts to increase adhesion–cytoskeletal coupling on LN, we cultured growth cones under the different conditions, double stained for vinculin and MII (Figure 6, A–E), and then assessed the staining characteristics of vinculin spots (Figure 6, E and F). High NGF caused the staining intensity to increase on LN and decrease on FN (Figure 6E; *t* tests, $*p < 0.02$, $**p < 0.05$). The average length (largest dimension) of individual spots decreased on both substrates (Figure 6F). However, the total length of vinculin staining per growth cone remained roughly constant on LN (because the number of spots was higher) and decreased on FN. High NGF also caused a redistribution of spots in growth cones on LN such that the majority of spots were close to the leading edge. Live imaging of GFP-vinculin in high NGF revealed that the lifetimes of vinculin spots were shorter on LN than with FN.

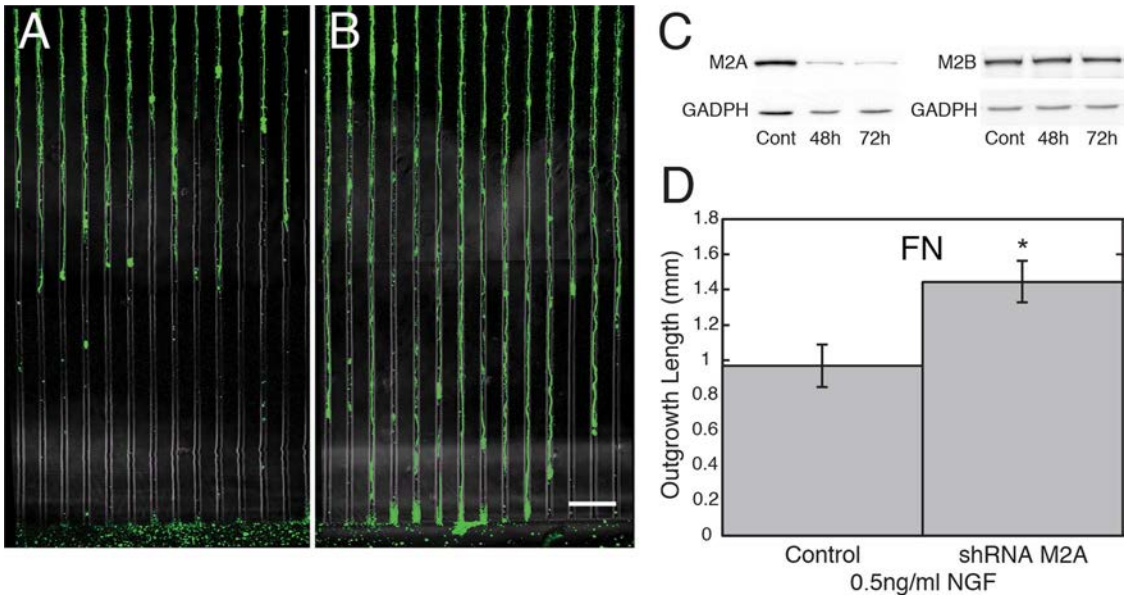

FIGURE 4: Partial knockdown of MIIA expression causes an increase in the axon outgrowth rate on FN. DRG neurons were plated in the central well of a Campenot chamber and infected with an adenovirus vector 2 h after plating for 5 h in defined medium (without serum) and then allowed to recover in normal medium for 2 h. Vectors contained inserts to express control (scrambled) or MIIA knockdown shRNA (four chambers per dish, half receiving one vector and half the other). Cells were cultured for another 96 h in low NGF and then fixed and stained for neurofilament H (green) and MIIA (not shown). Axon outgrowth lengths were smaller (A) for cells expressing the control shRNA than (B) for cells expressing MIIA knockdown shRNAi. Bar, 100 µm. (C) Immunoblots showing that MIIA knockdown shRNAi causes a decrease in the levels of the MIIA heavy chain but not MIIB heavy chain. (D) Average axon length was greater for cells expressing the knockdown shRNAi than for cells expressing the control shRNAi (*t* test, (*$p < 0.02$). $N = 28$ each (from two separate wells). Based on the fluorescence intensity level of immunostaining for MIIA normalized to neurofilament staining, there was partial knockdown of the level of MIIA in distal axon segments for all experiments at 96 h. For cells growing on FN in low NGF, the reduction was 44% (CT = 100 ± 4 vs. KD = 66 ± 8% of CT). $N = 20$ and 32. Similar tests were performed for cells growing on LN and also in high NGF. At 96 h, the only significant increase in axon outgrowth occurred for cells growing on FN in low NGF, as shown (experiment repeated for all conditions at 96 h and for cells on FN at 112 h).

On LN, 40% of the spots that could be followed in time-lapse recordings appeared and then disappeared during the 5-min recordings (average lifetime, 44 ± 7 s), whereas on FN, >95% of the spots that could be unambiguously followed in time-lapse recordings persisted the entire length of the recording (5 min). In the remaining 5%, we only caught either the appearance or disappearance of the spots. Although we were unable to calculate the lifetimes on FN, the average has to be considerably greater than the length of the recordings (300 s).

A localized increase in the amount of vinculin staining (number of spots and intensity per spot) combined with intermediate rates of turnover is consistent with an increase in adhesion–cytoskeletal coupling, which has been shown to slow retrograde flow in nonneuronal cells (Gupton and Waterman-Storer, 2006). Thus NGF may cause slowing of retrograde flow on LN by inducing increased peripheral adhesion–cytoskeletal coupling. This possibility is supported by the observation that growth cones appear to displace beads embedded in LN-coated flexible substrates to a greater degree in high NGF than in low NGF (Figure 7, A and B).

The results from the experiments using MIIB KO cells provide further support for our previous findings that MIIB is primarily responsible for the axonal growth-promoting effects when cells are on LN. However, MIIB activity does not seem to be strongly regulated by NGF. Thus, how does MIIB promote faster outgrowth in response to NGF? If adhesion–cytoskeletal coupling is important for the MII-dependent regulation of restraint and outgrowth, then MII (mainly MIIB) may act to enhance formation of adhesion complexes (Ketschek *et al.*, 2007) and/or organize actin on LN. Consistent with this possibility, treatment with blebbistatin disrupted normal growth cone morphology and retrograde flow and caused changes in the size and distribution of vinculin-positive adhesion spots on both LN and FN. The spots appeared to be reduced in size (intensity) and more randomly distributed. The smaller spots on LN were too small (diffraction limited) to allow accurate measurement of size (not shown, but the appearance was essentially the same as in KO growth cones treated with blebbistatin; see Figure 3, E and F), and the decrease in size on FN was significant (Figure 6F; ANOVA, ***$p < 0.001$). Ketschek *et al.* (2007) also observed decreased vinculin staining in response to blebbistatin treatment for cells on LN. If adhesion were the only factor responsible for the growth-promoting role of MIIB, then blebbistatin would have the same effect on cells growing on FN. However, this was not the case. This suggests that MII may have isoform-specific roles, depending on the growth substrate.

Perturbing adhesion–cytoskeletal coupling using tailless vinculin increases retrograde flow rates on LN and decreases outgrowth

To test directly whether an increase in adhesion-cytoskeletal coupling is responsible for the decrease in retrograde flow on LN, we overexpressed either GFP–tailless vinculin or wild-type (Wt) GFP-vinculin. The tailless vinculin protein lacked an actin-binding domain

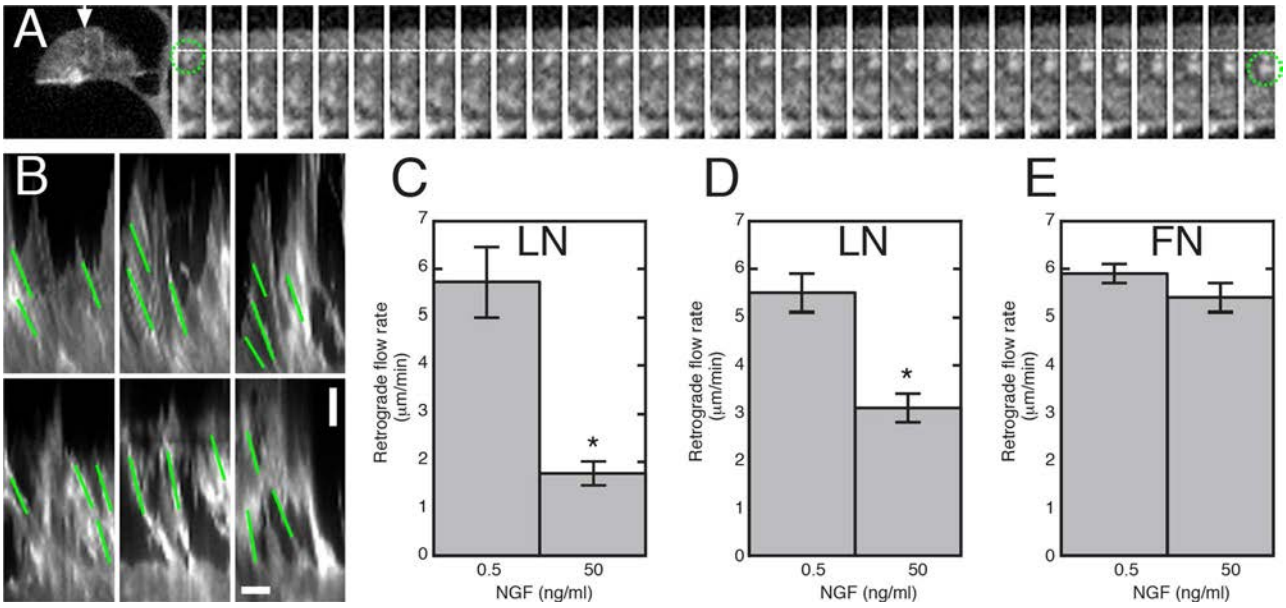

FIGURE 5: NGF negatively regulates growth cone retrograde actin flow on LN. (A) An example of retrograde flow analysis using tdEOS-actin spot (green circle) tracking at 1-s intervals. (B) Composite showing kymographs at different areas of a growth cone expressing GFP-LifeAct in high NGF (top) and another in low NGF (bottom). The change in distance (*y*- axis; bar, 1.6 μm) over time (*x*-axis; bar, 0.8 m; slope indicated by green lines) was used to calculate the retrograde flow rate. (C) Quantitation of retrograde flow using tdEOS-actin spot analysis. The rate of retrograde flow slows significantly in high NGF (*t* test; $*p < 0.001$). *N* = three to six spots per growth cone, eight growth cones per category. (D) Retrograde flow rates calculated from kymographs of growth cones expressing GFP-or Ruby-LifeAct. Similar to the spot analysis, the rate of retrograde flow slows significantly in high NGF. However, the slowing is less dramatic than that observed using spot analysis of tdEOS-actin. To verify that the kymograph analysis was valid, individual spots were also tracked (minimum three frames). The average rates of individual spots did not differ significantly from the rates obtained by kymograph analysis under the different conditions. Data represent average flow rates from three experiments (one GFP-LifeAct, two Ruby-LifeAct). *N* = 56, 50, 40, and 55 for the respective categories. Retrograde flow was significantly slower in high NGF on LN (*t* test; $*p < 0.002$). (E) Quantitation of peripheral (i.e., distal to transverse bundles) retrograde flow in growth cones on FN using kymograph analysis. The average flow rates in low and high NGF were not significantly different (*t* test; $p > 0.2$).

(Grashoff *et al.*, 2010), so it could not bind actin and therefore should disrupt adhesion–cytoskeletal coupling. We measured retrograde flow rates ~20 h or longer after transfection of cells on the two substrates. The retrograde flow rates were significantly higher in growth cones of cells expressing tailless vinculin than in controls or in growth cones of cells expressing the Wt vinculin on LN (Figure 8A; ANOVA; $*p < 0.001$). No significant difference in retrograde flow rates was observed on FN (Figure 8B; ANOVA, $p > 0.2$). Expression of tailless vinculin resulted in dramatically slower outgrowth for cells growing on LN in low or high NGF (Figure 8C; *t* tests, $*p < 0.0001$, $**p < 0.001$). Expression of tailless vinculin decreased outgrowth rates uniformly across all conditions tested (CT and MIIB KO on LN or FN, high or low NGF; Figure 8D; ANOVA, $p = 0.2$). The axon outgrowth rates were close to the rates observed for cells grown on PLO or PEI. The lack of a stimulatory response to NGF or the substrate in both CT and MIIB KO cells suggests that tailless vinculin was disrupting adhesion–cytoskeletal coupling. Thus we reasoned that overexpression of Wt vinculin may induce faster axon elongation in cells grown in low NGF because of increased adhesion–cytoskeletal coupling.

Overexpression of Wt vinculin increases outgrowth rates in low NGF

To test this possibility, we overexpressed Wt vinculin in cells growing on LN and then measured axon outgrowth after overnight exposure to either low NGF or high NGF. Outgrowth rates in high NGF were the same for cells expressing Wt vinculin, untransfected cells in the same culture, and cells in the same culture expressing tdTomato (vector control; Figure 8E). However, outgrowth rates in low NGF were significantly faster for cells expressing Wt vinculin than for untransfected cells or cells transfected with tdTomato growing in the same culture (*t* test, $*p < 0.05$). Thus overexpression of Wt vinculin can compensate for low NGF when cells are grown on LN. This supports the idea that cells growing on LN substrates primarily respond to higher levels of NGF by increasing the amount of vinculin that is available for formation of adhesions.

Overexpression of the GFP–tailless vinculin produced relatively large, stable spots in growth cones on LN (Figure 9A) and slowed outgrowth, but coexpression of tdTomato-EB3, an end-binding protein that associates with dynamic microtubules (Stepanova *et al.*, 2003), resulted in decreased lifetimes compared with control cells (Figure 9, B and C; *t* test, $*p < 0.001$). This indicates that disruption of adhesion–cytoskeletal coupling decreases persistent dynamic microtubule polymerization into the growth cone periphery.

Retrograde actin flow regulates dynamic microtubule advance and correlates with elongation rate

To assess whether the decreased retrograde flow rate on LN corresponds to more frequent dynamic microtubule advance, we transfected neurons with GFP-EB3 (Figure 10A). On LN, addition of NGF

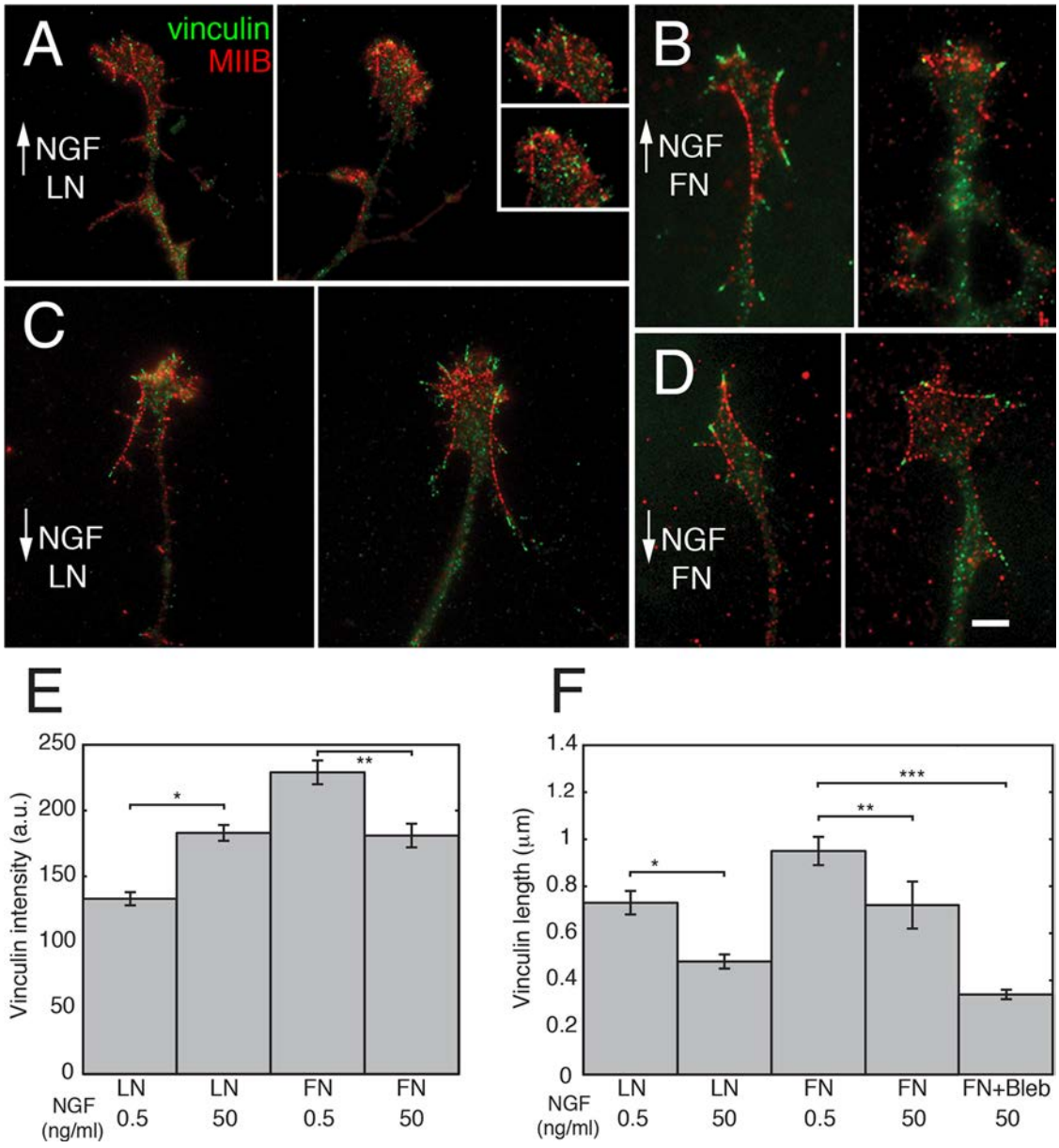

FIGURE 6: Substrate composition and NGF concentration affect the size and enrichment of vinculin aggregations at focal adhesion sites of growth cones. Immunofluorescence staining of MIIB (red) and vinculin (green) for (A) LN + high NGF, (B) FN + high NGF, (C) LN + low NGF, and (D) FN + low NGF. Bar, 10 μm. (Note that image brightnesses were adjusted for display.) (E) Vinculin staining intensity on LN increases significantly with an increase in NGF concentration (*t* test; $*p < 0.02$). Conversely, the staining intensity on FN decreases significantly with the higher level of NGF (*t* test; $**p < 0.05$). *N* = 12, 14, 16, and 28 growth cones per category (from three experiments). (F) Focal complex length identified by vinculin staining significantly decreases with increasing NGF concentration on both substrates (LN and FN; *t* test, $*p < 0.01$ and $**p < 0.02$; *N* the same as in E). However, the total length on LN was about the same due to an increase in the number of vinculin-positive spots in the higher NGF. On FN, the total length decreased by ~50% because the total number of spots as well as size decreased with the higher NGF. Blebbistatin treatment caused a further decrease in size on both substrates. This change was significant on FN (ANOVA; $***p < 0.001$; the small sizes on LN prevented accurate measurements). Blebbistatin treatment also randomized the distribution of spots in most growth cones. They were no longer concentrated on the periphery.

increased both the number of GFP-EB3 spots at the leading edge of the growth cone in a given time period (penetration; *t* test, $*p < 0.001$) and the length of time that GFP-EB3 spots could be tracked in peripheral protrusions (lifetime; Figure 10, B and C, and Supplemental Movies S1 and S2; *t* test, $*p < 0.001$). On FN, the effect of NGF was less dramatic, but the trend was the same: GFP-EB3 spots appeared to penetrate more deeply and had a longer lifetime (*t* test, $**p < 0.01$). The degrees of dynamic microtubule penetration and persistence were maximal on LN in high levels of NGF, the same conditions under which axon elongation was fastest.

To confirm this finding (and rule out any potential artifacts related to short-term [5 min] time-lapse imaging of EB3 spots), we fixed neurons grown under the same conditions, triple labeled the cells with antibodies to MII (A or B) and tyrosinated tubulin and

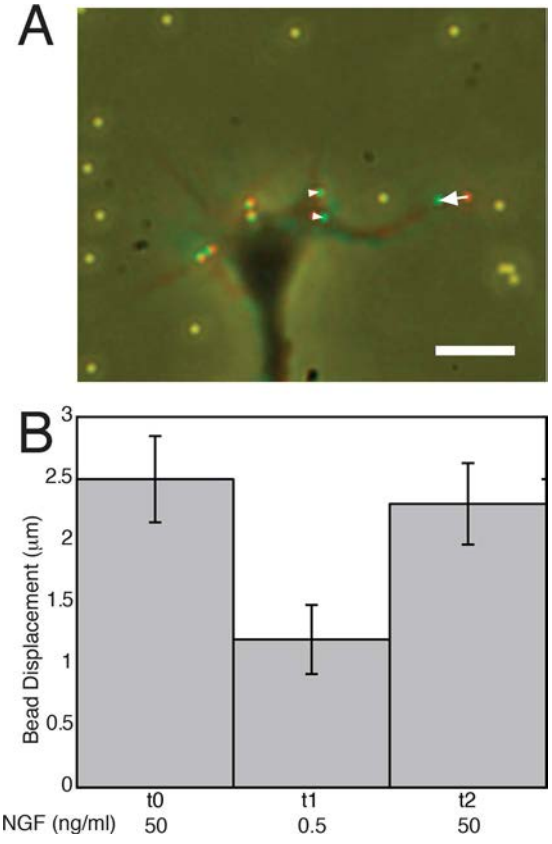

FIGURE 7: NGF increases traction force pulling on LN. (A) DRG neurons were grown on flexible substrates coated with LN containing embedded beads to measure changes in traction forces. Red-green overlay indicates the relative bead displacement (arrowheads, arrow) over time. Filopodia were generally associated with greater displacements. Note that beads far from the growth cone are yellow, indicating no displacement. Bar, 10 μm. (B) Lowering the NGF concentration (t1) appears to cause a decrease in the average maximum displacement of the beads as measured over time for the same growth cones. Returning to high NGF concentration (t2) caused the displacement to increase again as followed over time. Each time period corresponded to an observation period of 30 min.

rhodamine phalloidin to label F-actin, and then measured the distances of microtubule profile ends that projected into the actin-rich periphery from the leading edge in growth cones. The variance of measured distances (in micrometers) was lower for growth cones in high NGF than for those in low NGF, but this difference was significant only for growth cones on LN (LN, 50 ng/ml NGF, variance 2.3, $N = 58$; 0.5 ng/ml NGF, variance 14.8, $N = 27$; difference was significant by a two-tailed F-test of the variance between two samples; FN, 50 ng/ml NGF, variance 2.9, $N = 21$; 0.5 ng/ml NGF, variance 3.1, $N = 22$, difference nonsignificant). This is consistent with the data showing that NGF induced a large change in density and lifetime of EB3 spots on LN but not on FN. As expected, the variance is inversely related to the density and lifetime of EB3 spots.

Expression of GFP–tailless vinculin also decreased the lifetime and penetration of tdTomato-EB3 into the periphery of growth cones (Figure 9, A–C, and Supplemental Movie S3). Growth cones on LN grew slowly after treatment with blebbistatin, but tdTomato-EB3 comets appeared to penetrate the periphery to a greater extent than in high NGF (Figure 11A). To obtain quantitative data on the degree of penetration, we measured the frequency of leading-edge interactions and EB3 spot lifetimes in growth cones on LN. Blebbistatin treatment caused the frequency of interactions with the leading edge to increase compared with controls (Figure 11B and Supplemental Movie S4; t test, $^*p < 0.03$) and also sometimes caused "deflection," that is, the redirection of polymerizing microtubules such that they traveled along the perimeter of the leading edge and occasionally back toward the central domain (Figure 11A). Blebbistatin treatment also caused a decrease in EB3 spot lifetimes (Figure 11C; t test; $^*p < 0.001$). The greater interaction with the leading edge despite shorter lifetimes suggests that blebbistatin treatment decreases restraint (i.e., slows retrograde flow; Medeiros *et al.*, 2006), but microtubule ends are not stabilized upon reaching the periphery.

NGF causes reorganization of MIIA-dependent actin bundles on LN

Whereas one effect of NGF was to increase the frequency and persistence of dynamic microtubule entry into the periphery of growth cones on LN, we also observed that the GFP-EB3 comets were less likely to curve and move off-axis (when MII was active). This suggests that NGF may also cause an increase in microtubule bundling. MII has been shown to play a role in microtubule bundling in *Aplysia* growth cones (Burnette *et al.*, 2008). Immunofluorescence images of growth cones on LN labeled for MIIA and dynamic microtubules (Figure 12, A and B) suggest that MIIA partially reorganizes upon NGF stimulation. The greatest difference is observed between rapidly advancing growth cones on LN in high NGF and slowly advancing growth cones on FN in low NGF (Figure 12, C and D). In rapidly advancing growth cones, MIIA-associated transverse actin bundles at the growth cone leading edge decrease (quantitation is shown in Figure 12, E and F), whereas bundles roughly parallel with the lateral edges of the cone increase. This added lateral restraint may restrict microtubule splaying, causing microtubule advance to be directed more toward the leading edge.

NGF reduces transverse actin bundling at the leading edge on FN

To determine whether bundling was reduced by NGF treatment, we compared the distribution of MIIA and MIIB in growth cones on LN and FN (Figure 12, E and F). NGF reduced the number of arc-like, MIIA-associated transverse bundles running parallel to the leading edge of the growth cone (and orthogonal to the direction of retrograde flow) for growth cones on FN (Bernoulli distribution mean and variance formulas, 95% confidence interval, one-tailed case). Double labeling indicated that many of these bundles (~80%) also contained MIIB. However, we believe that their formation may depend primarily on MIIA. The bundles still formed in MIIKO cells growing in low NGF and were rarely seen after MIIA knockdown. Similar effects were observed on LN but were less prominent (Figure 12E). MIIB-associated bundles showed a similar relationship and trend but were less frequent on FN (Figure 12F). On FN in low NGF, MIIA-dependent actin bundles formed an increase in transverse bundles that contributed to a "cage-like" structure around the perimeter of the growth cone. This structure was anchored to vinculin-positive adhesion sites and restricted dynamic microtubule extension (Figure 12D). Actin bundles running parallel to the lateral edges or in filopodia were less affected and generally closer to the edges than those on LN, which may allow greater microtubule splaying.

DISCUSSION

Local application of NGF has both trophic and tropic effects on sensory and sympathetic axons, inducing changes in speed and

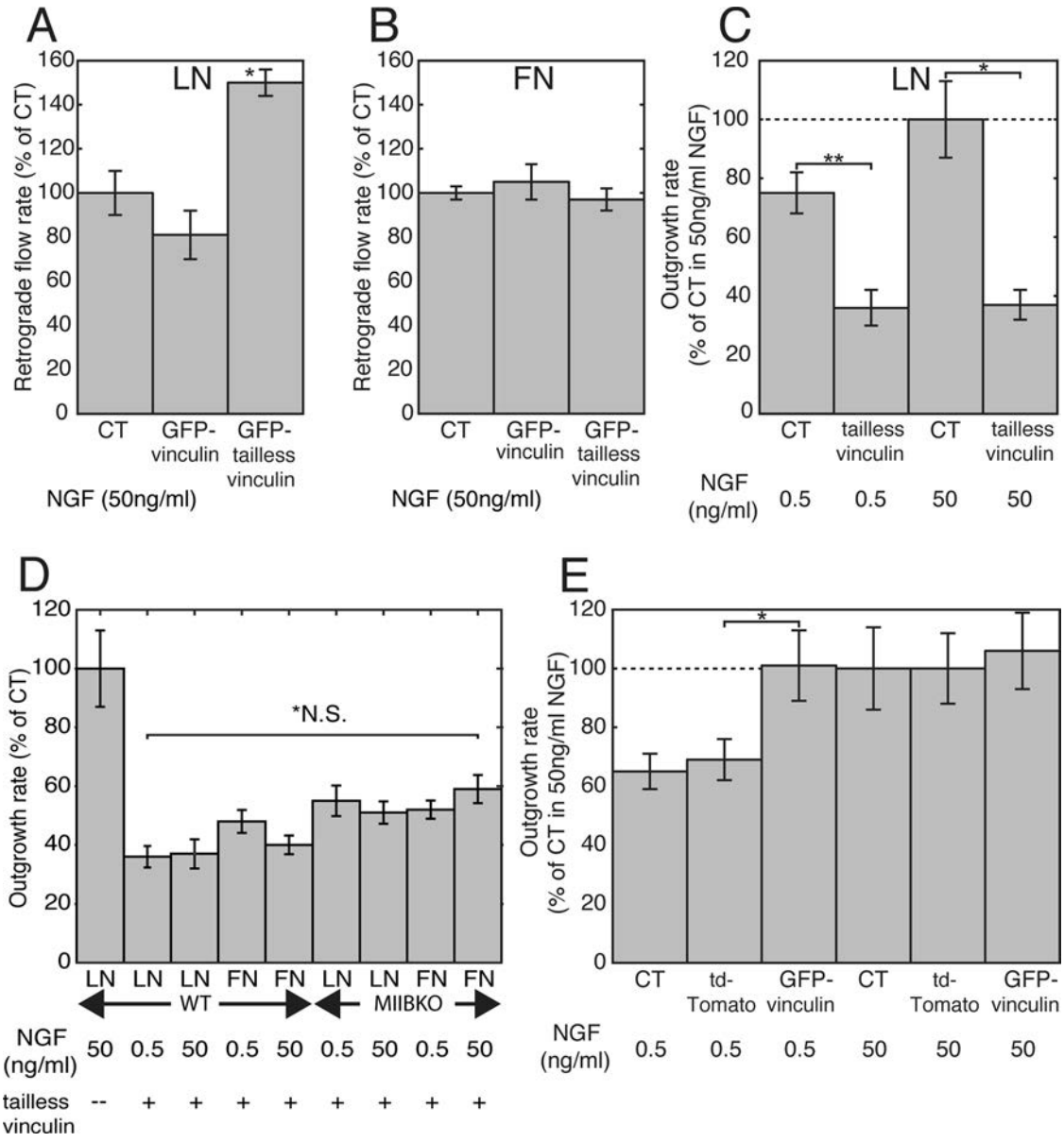

FIGURE 8: Overexpression of tailless vinculin results in faster retrograde flow and slower outgrowth on LN, whereas overexpression of CT vinculin in low NGF stimulates outgrowth similar to NGF. (A) Retrograde flow was significantly faster in cells expressing GFP–tailless vinculin and Ruby-LifeAct than in cells transfected with only Ruby-LifeAct (CT) or GFP-vinculin and Ruby-LifeAct (ANOVA; *$p < 0.001$). $N = 67$, 32, and 67. (B) Expression of GFP–tailless vinculin did not affect retrograde flow rates on FN (ANOVA, $p > 0.02$). Expression of GFP–tailless vinculin causes axon outgrowth to slow on LN. Conversely, overexpression of CT GFP-vinculin causes faster outgrowth in low NGF. (C) Cultures transfected with a construct for GFP–tailless vinculin were grown overnight (14 h) in either high or low NGF on LN and then fixed. Comparison of axon lengths of transfected and untransfected cells from the same culture. The differences were significant by *t* test (*$p < 0.0001$ and **$p < 0.001$). $N = 16$ and 12 each (for high and low NGF, respectively). A second experiment gave the same result. (D) Expression of tailless vinculin decreased outgrowth rates independent of phenotype, substrate composition, or NGF concentration. ANOVA, *$p = 0.2$. $N = 12$ (or greater) per category. (E) Expression of CT GFP-vinculin had no effect on outgrowth in normal NGF on LN but increased the rate of outgrowth compared with untransfected control cells (CT) or cells transfected with vector only (tdTomato) plated in the same culture in low NGF. The difference between the vector control and GFP-vinculin was significant by *t* test (*$p < 0.05$). $N = 19$ each. A second experiment gave the same result.

direction, respectively (Gundersen and Barrett, 1980; Campenot, 1982a,b). In this study, we sought to understand how NGF stimulates faster axonal elongation and whether it does so in a manner that is fundamentally different from how it influences guidance. It was shown that changes in growth rate (i.e., trophic effects) can account for turning in shallow gradients but not in steep gradients (Mortimer *et al.*, 2008; Mortimer *et al.*, 2010). Does NGF exert trophic and tropic effects through multiple mechanisms, as this previous work suggests, or can it be explained by a single mechanism of action? To address this question, we first examined whether inhibition of MII blocked the growth cone response to NGF. Whereas inhibition of MII clearly blocked the response to NGF, further tests

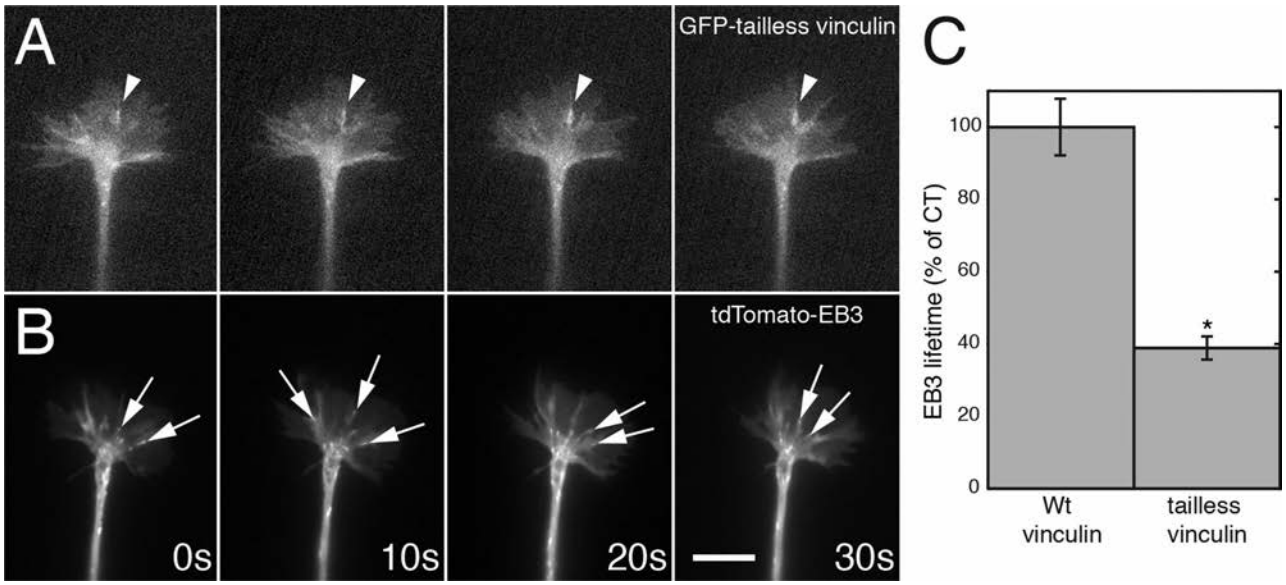

FIGURE 9: Expression of GFP–tailless vinculin alters retrograde flow and EB3 penetration into the growth cone periphery. (A) Sequence showing a growth cone expressing GFP–tailless vinculin (10-s intervals). Relatively large vinculin spots (arrowhead) formed and persisted. (B) tdTomato-EB3 dynamics in the same growth cone (taken sequentially). EB3 comets (arrows) rarely penetrate to the actin-rich periphery of the growth cone. (C) Lifetimes of EB3 spots were also significantly reduced by tailless vinculin expression (*t* test, $*p < 0.001$). Bar, 14 μm.

revealed that MII plays multiple outgrowth-dependent roles that are isoform specific.

In previous studies, we found that MII is necessary for the stimulative and repulsive effects of LN and Sema3A, respectively (Turney and Bridgman, 2005; Brown *et al.*, 2009), and others showed that MII regulates the outgrowth of minor processes and the development of polarity in multipolar neurons (Kollins *et al.*, 2009). The common requirement for MII points to the possibility of a single mechanism underlying directed outgrowth. In this study, we found that inhibition of MII eliminated faster outgrowth in response to an increase in NGF. Of interest, the rate of axon outgrowth decreased on LN (in high NGF) and increased on FN (in low NGF). Thus MII is required for stimulation of axon outgrowth by NGF but has different roles on the two substrates. From this result, we were motivated to investigate whether the roles of MII are complementary, as they appear to be, or whether MII can be understood to be contributing to different components that have the same basic function in the mechanism.

Our prior work produced a finding directly relevant to this question. We observed that MII affected axon outgrowth in a complementary manner on LN versus PLO (Turney and Bridgman, 2005). Blebbistatin treatment caused mouse SCG axon outgrowth rates to increase on PLO. Conversely, loss of MIIB function resulted in slower axon outgrowth on LN. Our interpretation was that the change in role of MII from inhibiting axon outgrowth on PLO to enhancing outgrowth on LN was likely due to LN-specific support for integrin activation, adhesion formation, and traction forces. A subsequent study confirmed these results, showing that inhibition of MII caused chick DRG axon outgrowth rates to decrease on LN and increase on PL (Ketschek *et al.*, 2007). Further, this study concluded that MII inhibits outgrowth on PL through restraint of microtubule advance and promotes outgrowth on LN through its association with integrin-mediated adhesions.

If substrate support for integrin activation and adhesion formation determines the role of MII, as suggested, then one might expect the role of MII to be the same on LN and FN. However, as mentioned, we found that inhibition of MII caused axon outgrowth to slow down on LN and speed up on FN in high and low NGF, respectively. Thus we were then motivated to discover 1) why NGF stimulates faster outgrowth on FN but not on PLO (MII inhibits outgrowth on both substrates), 2) why the role of MII is different on LN from that on FN (both substrates support integrin-mediated adhesions), and 3) whether MII has the same basic function on LN as on FN. The role of MII on LN was not fully elucidated in past studies. Moreover, the role of MII on FN and the effect of changes in NGF had not been previously addressed. As described later, our new findings indicate that NGF regulates a different actomyosin restraint process on LN than on FN.

MIIA and MIIB have separate functional roles in regulating NGF-stimulated axon outgrowth on different substrates

Inhibition of MII in an isoform-specific manner revealed that NGF stimulation differentially requires MIIA and MIIB on FN and LN, respectively. We determined that this substrate dependence is due to MIIA and MIIB having separate functional roles. Our evidence points to MIIA driving the formation of transverse actin bundles anchored (at their ends) by vinculin-dependent adhesions and MIIB affecting peripheral rearward (radial) actin network flow. We found that vinculin-dependent adhesions are smaller and less stable but more numerous on LN than on FN. Our view is that large, stable adhesions are required for the assembly of actin bundles, whereas the small, transient adhesions support tethering to the rearward-flowing actin network in the periphery. We found that NGF primarily causes down-regulation of MIIA activity on FN and an increase in total vinculin-dependent cytoskeletal coupling on LN.

Although it is known that substrates composed of extracellular matrix components can modulate the motility and growth responses of neurons to growth factors and guidance cues and that the changes in behavior are associated with RhoA activity, the underlying mechanisms linking RhoA activity to growth cone motor output

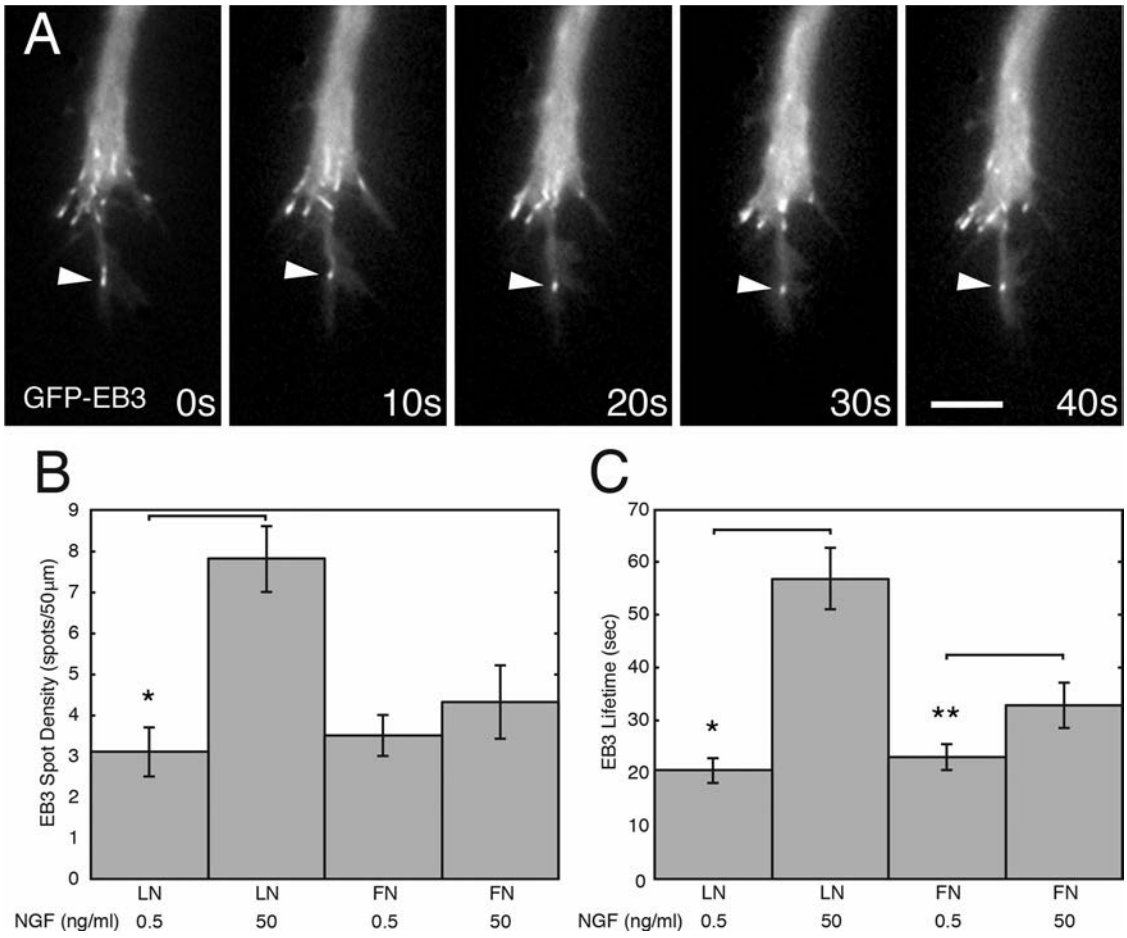

FIGURE 10: Substrate composition and NGF concentration influence microtubule dynamics. (A) Microtubule dynamics monitored using GFP-EB3. A time-lapse sequence taken from a growth cone on LN in high NGF. An EB3 comet (arrowhead) entering a peripheral protrusion is highly persistent (frame intervals shown are 10 s). (B) The density of GFP-EB3 or tdTomato-EB3 spots (comets) increased near the leading edge of growth cones on LN in high NGF compared with low NGF. Density was computed for spots on each frame from movies (40 frames total, 5-s interval) within 5 µm of the leading edge and across a contour of 50 µm. The average density over time was calculated for each growth cone (*t* test, LN, $*p < 0.001$). $N = 7$ per category. (C) EB3 lifetimes increased near the leading edge of growth cones on LN and FN in high NGF. The same movies used for B were analyzed for EB3 spot lifetimes. A minimum of 16 spots per growth cone was analyzed (*t* test; LN, $*p < 0.001$; FN, $**p < 0.01$).

remain largely unresolved (Gomez and Letourneau, 1994; Dontchev and Letourneau, 2002; Liu *et al.*, 2002; Gehler *et al.*, 2004). Here we found that inhibition of RhoA using C3 transferase mimicked the effect of NGF-induced inactivation of MIIA (Figure 13). The resulting increase in axon outgrowth rate was greater on FN than on LN, consistent with MIIA-dependent restraint playing a greater role on FN.

The maximal axon outgrowth rates supported on LN are linked to the function of MIIB. Elimination of MIIB (MIIB KO) caused axon outgrowth rates to decrease on LN. In addition, the stimulative effect of NGF was significantly reduced (Figure 13). Previously we showed that MIIB KO cells on LN had weaker traction forces, less persistent (i.e., more undirected) growth cone advance (Bridgman *et al.*, 2001), and a higher rate of retrograde actin flow (Brown and Bridgman, 2003). These results suggest that vinculin-positive adhesions that form in the absence of MIIB are not associated with normal levels of cytoskeletal coupling. In nonneuronal cells, it is believed that the interplay between actomyosin and focal adhesion dynamics results in a specific balance between adhesion and contraction and that this balance produces maximal migration velocity (Gupton and Waterman-Storer, 2006). Thus the main role of MIIB may be to maintain this balance through its effects on retrograde flow and adhesion–cytoskeletal coupling. Our findings indicate that MIIB strengthens the tethering of the peripheral actin network to adhesion sites on LN and that the combination of tension-induced maturation of adhesions (Pasapera *et al.*, 2010) and NGF stimulation causes an increase in vinculin levels at adhesions that correlates with greater adhesion–cytoskeletal coupling. The result is a slowing of retrograde flow that allows dynamic microtubules to enter the growth cone periphery more efficiently. The slowing is also intrinsically linked to generation of growth cone traction forces (Bridgman *et al.*, 2001; Chan and Odde, 2008), so a question is whether traction force pulling contributes significantly to the faster elongation seen on LN. In previous work, we showed that low concentrations of nocodazole that dampened dynamic microtubule polymerization into the growth cone periphery profoundly inhibited the rate of axon elongation (but not increases in axon volume; Rochlin *et al.*, 1996). Our view is that microtubule advance is required for growth cone advance and therefore controls the elongation rate. More work is needed to support this idea.

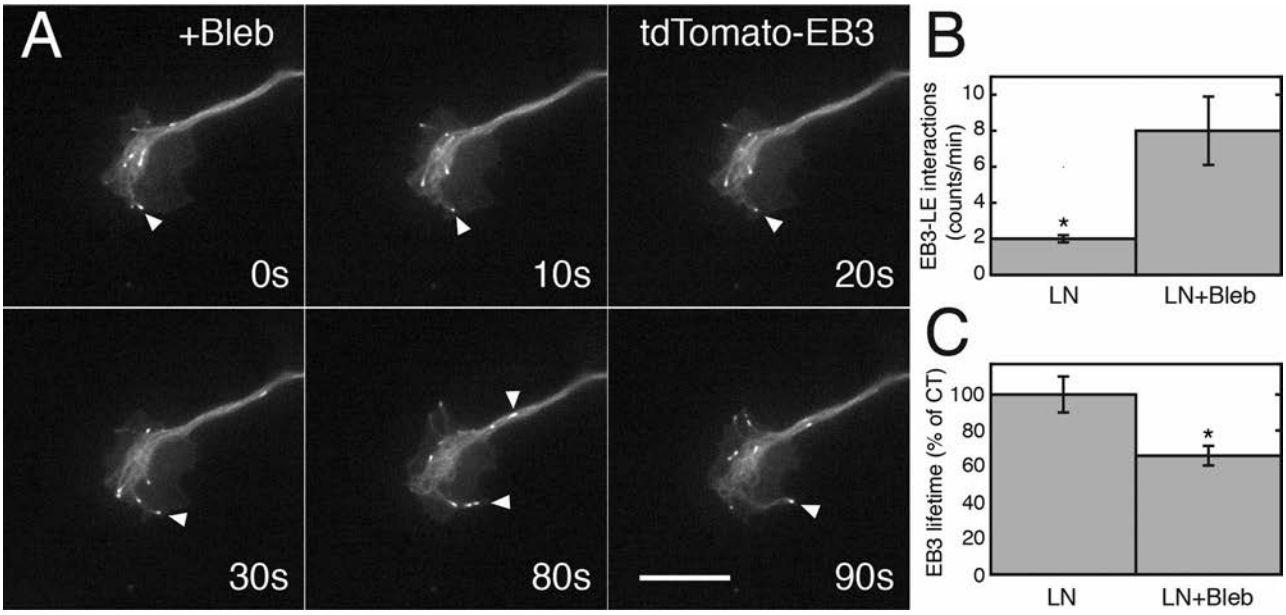

FIGURE 11: Blebbistatin treatment leads to a higher rate of microtubule interactions with the leading edge but shorter lifetimes. (A) Sequence showing tdTomato-EB3 dynamics in a growth cone 40 min after application of blebbistatin. EB3 comets (arrowheads) travel along the leading edge or occasionally travel rearward in the connecting axon. (B) Quantitative analysis of the frequency of EB3 comet–leading edge (LE) interactions. Blebbistatin significantly increases the frequency of LE interactions (*t* test, $*p < 0.03$). (C) Lifetimes of EB3 spots were also significantly decreased *t* test ($*p < 0.001$). Analysis was performed on movies (40 frames at 5-s intervals) of control ($N = 6$) and blebbistatin-treated ($N = 9$) growth cones from two experiments. Movies of blebbistatin-treated growth cones were taken within 3 h of treatment.

From the foregoing, we conclude that NGF induces faster axon outgrowth by decreasing MIIA-dependent transverse actin bundling (mostly on FN) and slowing MIIB-dependent retrograde network flow (mostly on LN). Both effects are consistent with reduced restraint of microtubule advance and correlate with a higher probability of microtubule entry into the actin-rich growth cone periphery. These results support and extend previous work showing that retrograde actin flow contributes to restraint of microtubule advance (Suter *et al.*, 2004; Lee and Suter, 2008). They also show that NGF regulates two actomyosin processes in sensory neurons.

The role of focal adhesion sites in axon outgrowth

Substrate adhesion and the activation and signaling of focal adhesion complexes and associated integrins greatly influence outgrowth and guidance (Letourneau, 1975; Brouns *et al.*, 2001; Mills *et al.*, 2003; Tucker *et al.*, 2005; Robles and Gomez, 2006). For instance, focal adhesion kinases regulate the formation of point contacts in growth cones with an efficiency that depends on the type of extracellular matrix substrate (Robles and Gomez, 2006), and integrin activation can affect Rac levels, which, in turn, regulate actin dynamics (Ng *et al.*, 2002). Our findings that NGF regulates substrate-dependent changes to vinculin-positive adhesion complexes and that these complexes are required for NGF stimulation of axon outgrowth are consistent with NGF influencing outgrowth rates through its effects on adhesion complexes. Although we did not study the upstream signaling pathways, it seems reasonable to assume that these adhesions overlap with point complexes that contain paxillin (Renaudin *et al.*, 1999; Robles and Gomez, 2006). The main point from our perspective is that the adhesion complexes represent a control point of the core MII-dependent mechanism through their ability to influence the rate of retrograde flow and/or actin filament bundling.

In summary, NGF stimulation of embryonic mouse sensory axon outgrowth is MII dependent. We found that NGF regulates two actomyosin processes: transverse actin bundling and peripheral retrograde (radial) network actin flow. These two processes oppose microtubule advance and differentially involve MIIA and MIIB, respectively. The large, stable, vinculin-dependent adhesions on FN promote MIIA-dependent transverse actin bundling, whereas the small, transient, vinculin-dependent adhesions on LN support tethering of MIIB-dependent peripheral retrograde actin network (slowing down its flow). NGF causes a large decrease in MIIA activity on FN and a significant increase in total vinculin-dependent coupling on LN. Restraint is decreased on both substrates, leading to more frequent entry of microtubules into protrusions and a corresponding increase in rate of advance. In the absence of MII activity, NGF fails to stimulate faster elongation, indicating the primacy of the role of actomyosin restraint in directed axon outgrowth.

MATERIALS AND METHODS

Cell culture and microfluidic devices

All animal procedures were performed in accordance with the Washington University School of Medicine Animal Care Committee's regulations. DRG neurons from embryonic day 13.5–14.5 control or MIIB KO mouse embryos (of either sex) were cultured either as explants or as dissociated cells. Neurons taken from wild-type and heterozygous embryos had the same outgrowth (Turney and Bridgman, 2005), and so controls were harvested from either in the same litter. Explants were plated on coated coverslips (0.1 mg/ml PLO + 20 μg/ml LN or 50 μg/ml FN), or, after being partially dissociated with a short (15 min) treatment with trypsin, they were placed in the open central wells of custom-designed microfluidic Campenot chambers. The microfluidic devices were made of polydimethylsiloxane. Each device

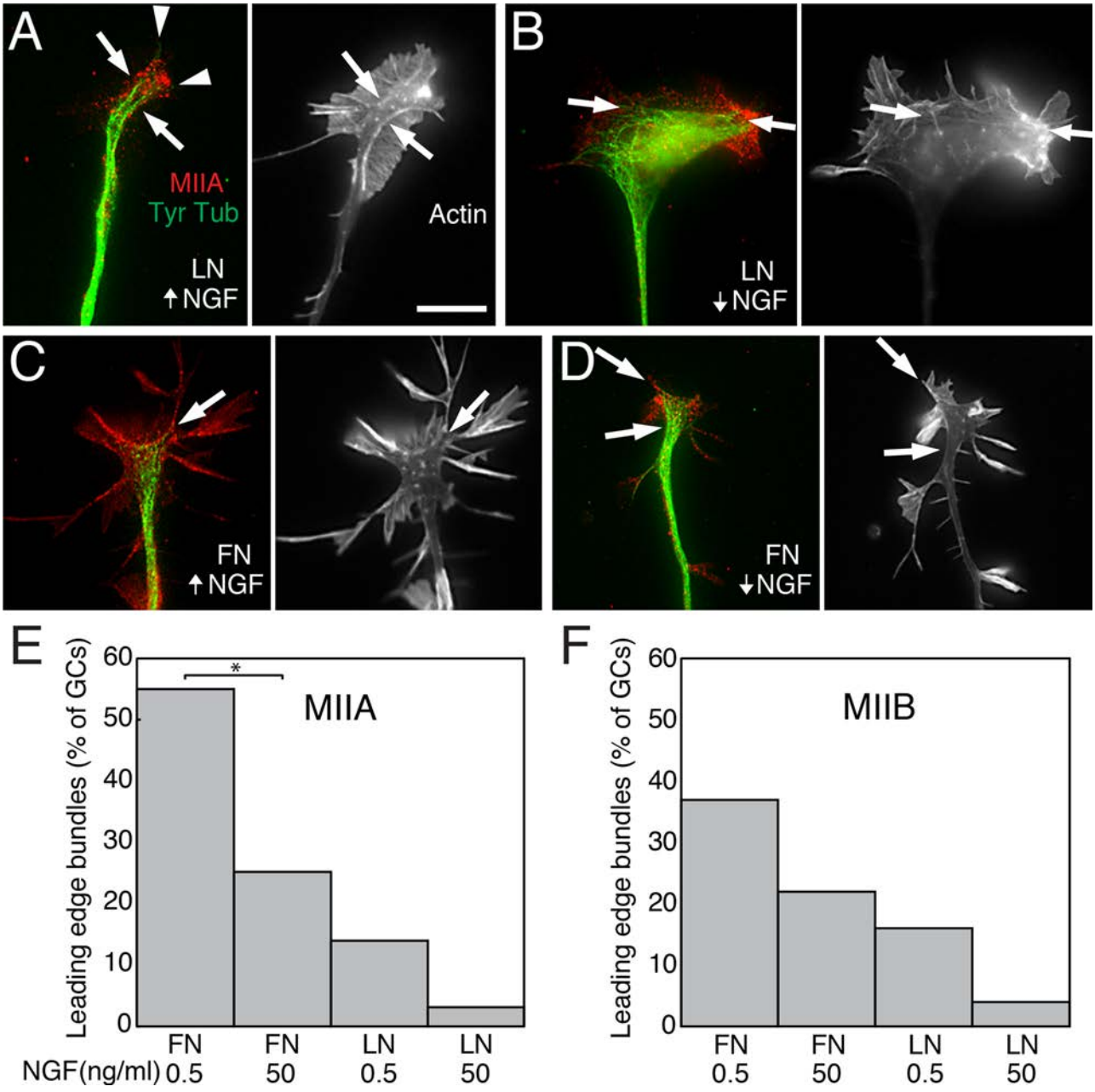

FIGURE 12: Substrate-dependent effect of NGF on the spatial distribution of MIIA, microtubules, and actin. (A) Growth cones on LN were grown overnight in high NGF, fixed, and stained with antibodies to MIIA and tyrosinated tubulin (left: red and green, respectively). Microtubules (arrows) occasionally appeared to be confined by MIIA (arrowheads). Actin was stained with rhodamine-phalloidin (right, grayscale). Distinct bright-stained bundles (arrows) partially colocalized with MIIA. (B) Growth cones on LN grown overnight in low NGF and then processed as in A. Microtubules (arrows) appeared to be frequently confined by MIIA-associated transverse actin bundles (arrows) near the leading edge. (C) Growth cones on FN grown overnight in high NGF and then fixed and stained as in A. MIIA bundles (arrows) associated with actin bundles (arrows) confined microtubules. (D) Growth cones on FN grown overnight in low NGF and then fixed and stained as in A. Transverse MIIA-associated actin bundles (arrows) appeared to frequently confine microtubules. Bar, 12 μm. (E) The percentage of growth cones that exhibited transverse MIIA bundles near the leading edge as a function of substrate and NGF concentration, detected by immunofluorescence. Increased concentrations of NGF decreased the frequency of bundles on both FN and LN substrates. However the difference was significant (asterisk) only on FN (based on Bernoulli distribution mean and variance formulas, 95% confidence interval, one-tailed case). In addition, the frequency of bundles was lower on LN than FN. (F) The trend is the same for MIIB bundles, but the frequency of MIIB bundles was generally lower on FN, and the differences did not reach a level of significance.

had four Campenot chambers, and one or two devices were bonded to a single glass coverslip. Regions of exposed glass were coated as mentioned. In each chamber, the cell body compartment (central well) was connected to the axon compartment via 10-μm-wide channels (a total of 50 per chamber). Campenot chambers rely on fluid pressure to prevent solutes in the axon compartment from reaching

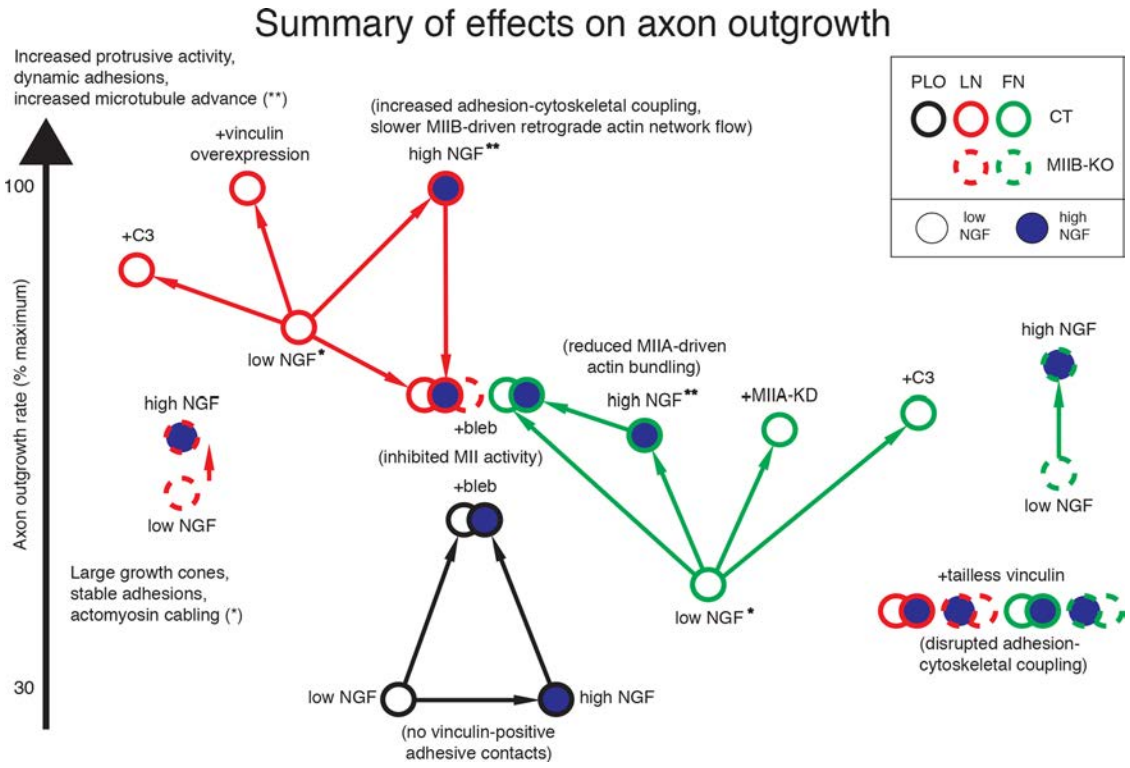

FIGURE 13: Summary diagram. Axon outgrowth rates of embryonic mouse DRG neurons (solid circles, CT; dashed circles, MIIBKO) as a function of growth substrate (LN, red; FN, green; PLO, blue), NGF concentration (low, open circles; high, blue-filled circles), and pharmacologic or genetic manipulation of MII activity (blebbistatin, C3 transferase, MIIA knockdown) and adhesion–cytoskeletal coupling (added expression of CT or mutant vinculin). Increasing the concentration of NGF induces faster axon outgrowth on LN and FN but not on PLO. Increasing NGF fails to stimulate faster axon outgrowth on LN and FN after blebbistatin treatment (inhibition of MII). The stimulative effect of NGF is mimicked by overexpression of CT vinculin on LN (increased adhesion–cytoskeletal coupling) and application of C3 transferase (inactivation of MIIA) or knockdown of MIIA expression on FN. Conversely, overexpression of tailless vinculin (disruption of adhesion–cytoskeletal coupling) greatly slows outgrowth and eliminates responsiveness to NGF. MIIBKO cells have axon outgrowth that is slower and more weakly NGF stimulated on LN than on FN. Inhibition of MII causes axon outgrowth rates to slow down on LN (in high NGF) and speed up on FN (in low NGF) and on PLO. Differences in axon outgrowth rates on LN and FN are MII and vinculin dependent, suggesting that the differences are not due to substrate adhesiveness. Together, these findings are consistent with MIIA and MIIB affecting axon outgrowth rates through separate adhesion-cytoskeletal coupling–dependent roles.

the cell body compartment or vice versa. In an open-well system, this is achieved by keeping the fluid level higher in one compartment. During virus exposure, the fluid levels were kept higher in the axon compartment. If an experiment required a low concentration of NGF in the axon compartment (e.g., allowing an increase in concentration later), we took special care to decrease the level of NGF in steps in order to avoid shocking the cells. In both compartments, the concentration was reduced to 5 and then 0.5 ng/ml using multiple rinses over 14 and 6 h, respectively. The low NGF concentration (0.5 ng/ml) supports survival of wild-type neurons and produces an outgrowth rate equivalent to that observed for neurons from BAX knockout mice in the absence of NGF (Liu *et al.*, 2002). Finally, we proceeded with the experiment, increasing the concentration of NGF to 50 ng/ml in the axon compartment only but maintaining a higher fluid level in the cell body compartment. The high concentration of NGF (50 ng/ml) is the standard or control concentration commonly used to stimulate growth of mouse DRG or superior cervical ganglion neurons. For chronic treatment of explants with different concentrations of NGF, blebbistatin, or C3 transferase, we first plated the explants in normal medium for 2 h and then grew the cells for another 16 h after changing medium. The cell-permeable C3 transferase was obtained from Cytoskeleton. Pilot experiments determined that 2 µg/ml was the lowest concentration that had a maximal effect on outgrowth. Experiments were repeated three times. Each experimental condition was typically run in duplicate along with two matching controls. Details of the microfluidics device will be described elsewhere.

Transfection

Cells fully dissociated by trypsin treatment (1 h) and trituration or partially dissociated with a short trypsin treatment were transfected using electroporation (Amaxa Nucleofector, Lonzo Group, Basel, Switzerland). The constructs GFP-MIIA, -MIIB, and -MIIC were gifts of Robert Adelstein (National Heart, Lung, and Blood Institute, National Institutes of Health, Bethesda, MD); tdEOS was a gift of Dylan Burnette; GFP-EB3 was a gift of Niels Galjart; GFP-LifeAct and Ruby-LifeAct were gifts of Dorothy Schafer; GFP-vinculin was a gift of Wolfgang Ziegler; GFP–tailless vinculin was from Addgene (plasmid 26020); and tdTomato-EB3 was a gift of Clare Waterman.

Reagents

NGF was from Harlan. Blebbistatin was from Calbiochem (Merck EMD Millipore, Darmstadt, Germany). Unless noted, all other reagents were from Sigma-Aldrich (St. Louis, MO).

Antibodies

Monoclonal antibody to human vinculin was from Sigma. Isoform specific antibodies to MIIA and MIIB were gifts of Robert Adelstein. Rat monoclonal antibody to tyrosinated tubulin was from Accurate Chemical. Chicken polyclonal antibody to neurofilament was from Covance. Monoclonal antibody to MLC was from Santa Cruz Biotechnology (Dallas, TX). The affinity-purified antibody to phosphorylated MLC was produced by R. B. Wysolmerski.

Imaging

Growing axons were imaged on a Zeiss (Carl Zeiss, Thornwood, NY) LSM 510 NLO microscope system (Axiovert 200 inverted stand) equipped with a motorized stage and a stage-mounted environmental chamber (PCO) or on an Olympus (Olympus America, Center Valley, PA) IX70 inverted microscope equipped with a sensitive charge-coupled device (CCD) camera (Sensicam; PCO-Tech, Romulus, MI), LED illumination (Prizmatix, Southfield, MI), and a custom environmental chamber. Some sequences were recorded on an inverted Leica microscope equipped with a Hamamatsu (Hamamatsu Corp., Bridgewater, NJ) ORCA-Flash 4.0 V2 CMOS camera. Extended time-lapse imaging on the Zeiss LSM 510 was performed using the Multi Time Series macro. Fixed cultures were imaged on either the Olympus IX70 or the Zeiss LSM 510. For explants, we measured the length of axons at positions around the perimeter of each explant, averaging six to eight per explant. For dissociated cells, measurements of axon lengths were obtained only for isolated axons that could be reliably traced.

shRNAi

Knockdown of MIIA was achieved using shRNAi constructs in adenovirus vectors tested for their isoform specificity in endothelial cells. Control constructs contained a scrambled sequence. Cells plated in the wells of microfluidic Campenot chambers were grown for 2 h and then exposed to virus (3×10^7 pfu/ml) for 5 h in defined medium (Neurobasal) supplemented with NGF (5 ng/ml). We then returned the cells to normal medium using several rinses.

Quantitative analysis of vinculin staining and retrograde flow rates

After fixation with 4% paraformaldehyde (electron microscopy grade) and permeabilization with 0.1% Triton, vinculin was stained using a monoclonal antibody (Sigma-Aldrich) and a fluorescein- or Alexa 488–conjugated secondary antibody. MIIA and MIIB were stained with isoform-specific polyclonal antibodies (Rochlin *et al.*, 1995). Diffraction-limited images were acquired using a 60×/1.4 numerical aperture (NA) oil-immersion objective on the Olympus IX70. We measured the size and intensity of vinculin staining at distinct adhesion complexes (≤2 × the background) on magnified digital images and then calculated the average size and intensity per growth cone. The longest dimension of each vinculin spot was measured. The width of small spots was close to the diffraction limit of the light microscope, so we did not attempt to measure areas. Intensity was measured as the maximum brightness per spot in a single in-focus image; the average brightness per growth cone was then obtained from multiple bright spots. For display purposes, brightness and contrast of images were adjusted using Photoshop (Adobe, San Jose, CA). The gamma setting was not altered. To measure retrograde flow rates, DRG neurons expressing tdEOS-actin or GFP- or Ruby-LifeAct were plated on LN or FN and grown overnight in low or high NGF. We used two methods to analyze rates: kymograph analysis of time-lapse images of growth cones (sequences of 40 images, one image every 5 s) and fluorescent spot analysis (up to 240 images taken at 1- or 5-s intervals). Kymographs were generated using single pixel-wide lines placed approximately parallel to the direction of actin retrograde flow (from time-lapse sequences) in multiple peripheral regions of growth cones using ImageJ (National Institutes of Health, Bethesda, MD). A minimum of four kymographs per growth cone was used to detect the change in actin over time and to calculate an overall average retrograde flow rate for each growth cone in the peripheral region (within 12 µm of the leading edge). To verify the accuracy of the kymograph analysis, we also tracked individual fluorescent spots in the time-lapse sequences taken at either 1- or 5-s intervals using a custom macro in ImageJ to measure the distances between points on successive images.

Quantitation of pMLC

Cells were fixed with cold methanol and stained with a monoclonal antibody to MLC and an affinity-purified antibody to pMLC. Green and red secondary antibodies were used, respectively. Cells were segmented by hand using IpLab, and backgrounds were subtracted from the green and red fluorescence images before performing ratiometric image analysis.

Quantitative analysis of isoform-specific pMLC

We acquired high-resolution two-dimensional images of growth cones using a high-NA oil immersion objective and low-light-sensitive CCD camera (see earlier description) on an epifluorescence microscope. The cells (expressing either GFP-MIIA or -MIIB) were fixed and stained with an antibody to pMLC (red fluorescent secondary). Images of red and green fluorescence had minimal bleedthrough. We performed colocalization analysis on images of individual growth cones using the JACoP plug-in in ImageJ. Blue and red scatterplots correspond to pixel-value distributions in low and high NGF, respectively (Figure 2, B and C).

Quantitative analysis of microtubule projections and MII bundles

DRG explants were grown overnight under four conditions: on LN or FN and in low NGF or high NGF. After fixation, growth cones were triple labeled for MIIA or MIIB, actin (using rhodamine phalloidin), and tyrosinated tubulin. To determine the relationship between microtubules and the leading edge, the distance between distal ends of microtubule projections into the actin-rich periphery and the leading edge were measured. The projections may represent one or more microtubules because we could not resolve closely aligned microtubules. In addition, we included only microtubules that had their distal axis oriented toward the leading edge. The orientation was defined by creating an axis aligned with the distal portion of the neurite (where it connected to the growth cone) and counting only the distal microtubule profiles that were oriented within ±30° of this axis. To analyze MII bundles, growth cones were scored for the presence of MIIA- or MIIB-transverse bundles at or near the leading edge (minimum of 20 growth cones in each category). To determine the contribution of the two isoforms to transverse bundles, in one experiment, we expressed GFP-MIIB in cells on LN growing in low NGF and then fixed and immunolabeled for MIIA.

Statistical analysis

Descriptive statistical analysis was carried out using Excel (Microsoft). The unpaired Student's *t* test was used to determine the significance between two groups. ANOVA was used to determine the significance between three or more groups. For post hoc analysis involving more than two groups, the Student's *t* test was used with the Bonferroni correction. The *F* test (two-tailed) was used to determine whether

the variances of two samples were equal or different. Statistical significance was defined as $p < 0.05$ or the 95% confidence interval.

ACKNOWLEDGMENTS

This research was supported by grants to P.C.B. from National Institutes of Health (R21 MH081260, R21 EB9776) and in part by the Bakewell Neuroimaging Core, an imaging facility supported by the Bakewell Family Foundation and National Institutes of Health Neuroscience Blueprint Interdisciplinary Center Core Grant P30 (NS057105) to Washington University. S.G.T. receives support from Jeff Lichtman and the Department of Molecular and Cellular Biology, Harvard University. R.B.W. was supported by grants from the National Institutes of Health (HL-090937, P20RR016440). The fabrication of microfluidics devices was performed in part at the Center for Nanoscale Systems, a member of the National Nanotechnology Infrastructure Network, which is supported by the National Science Foundation under award ECS-0335765. The Center for Nanoscale Systems is part of the Faculty of Arts and Sciences, Harvard University. R.M.R. received a postdoctoral fellowship (1 F32 NS60356-01) from the National Institutes of Health.

REFERENCES

Albers KM, Davis BM (2007). The skin as a neurotrophic organ. Neuroscientist 13, 371–382.

Bridgman PC, Dave S, Asnes CF, Tullio AN, Adelstein RS (2001). Myosin IIB is required for growth cone motility. J Neurosci 21, 6159–6169.

Brouns MR, Matheson SF, Settleman J (2001). p190 RhoGAP is the principal Src substrate in brain and regulates axon outgrowth, guidance and fasciculation. Nat Cell Biol 3, 361–367.

Brown ME, Bridgman PC (2003). Retrograde flow rate is increased in growth cones from myosin IIB knockout mice. J Cell Sci 116, 1087–1094.

Brown JA, Wysolmerski RB, Bridgman PC (2009). Dorsal root ganglion neurons react to semaphorin 3A application through a biphasic response that requires multiple myosin II isoforms. Mol Biol Cell, 20, 1167–1179.

Buck KB, Zheng JQ (2002). Growth cone turning induced by direct local modification of microtubule dynamics. J Neurosci 22, 9358–9367.

Burnette DT, Ji L, Schaefer AW, Medeiros NA, Danuser G, Forscher P (2008). Myosin II activity facilitates microtubule bundling in the neuronal growth cone neck. Dev Cell 15, 163–169.

Campenot RB (1982a). Development of sympathetic neurons in compartmentalized cultures. I. Local control of neurite growth by nerve growth factor. Dev Biol 93, 1–12.

Campenot RB (1982b). Development of sympathetic neurons in compartmentalized cultures. II. Local control of neurite growth by nerve growth factor. Dev Biol 93, 13–21.

Challacombe JF, Snow DM, Letourneau PC (1997). Dynamic microtubule ends are required for growth cone turning to avoid an inhibitory guidance cue. J Neurosci 17, 3085–3095.

Chan CE, Odde DJ (2008). Traction dynamics of filopodia on compliant substrates. Science 322, 1687–1691.

Coggeshall RE, Pover CM, Fitzgerald M (1994). Dorsal root ganglion cell death and surviving cell numbers in relation to the development of sensory innervation in the rat hindlimb. Brain Res Dev Brain Res 82, 193–212.

Dontchev VD, Letourneau PC (2002). Nerve growth factor and semaphorin 3A signaling pathways interact in regulating sensory neuronal growth cone motility. J Neurosci 22, 6659–6669.

Fischer M, Haase I, Wiesner S, Muller-Taubenberger A (2006). Visualizing cytoskeleton dynamics in mammalian cells using a humanized variant of monomeric red fluorescent protein. FEBS Lett 580, 2495–2502.

Gaese F, Kolbeck R, Barde YA (1994). Sensory ganglia require neurotrophin-3 early in development. Development 120, 1613–1619.

Gallo G, Lefcort FB, Letourneau PC (1997). The trkA receptor mediates growth cone turning toward a localized source of nerve growth factor. J Neurosci 17, 5445–5454.

Gehler S, Gallo G, Veien E, Letourneau PC (2004). p75 neurotrophin receptor signaling regulates growth cone filopodial dynamics through modulating RhoA activity. J Neurosci 24, 4363–4372.

Goldberg DJ, Burmeister DW (1986). Stages in axon formation: observations of growth of Aplysia axons in culture using video-enhanced contrast-differential interference contrast microscopy. J Cell Biol 103, 1921–1931.

Gomez TM, Letourneau PC (1994). Filopodia initiate choices made by sensory neuron growth cones at laminin/fibronectin borders in vitro. J Neurosci 14, 5959–5972.

Goold RG, Gordon-Weeks PR (2003). NGF activates the phosphorylation of MAP1B by GSK3beta through the TrkA receptor and not the p75(NTR) receptor. J Neurochem 87, 935–946.

Grashoff C, Hoffman BD, Brenner MD, Zhou R, Parsons M, Yang MT, McLean MA, Sligar SG, Chen CS, Ha T, Schwartz MA (2010). Measuring mechanical tension across vinculin reveals regulation of focal adhesion dynamics. Nature 466, 263–266.

Gundersen RW, Barrett JN (1980). Characterization of the turning response of dorsal root neurites toward nerve growth factor. J Cell Biol 87, 546–554.

Gupton SL, Waterman-Storer CM (2006). Spatiotemporal feedback between actomyosin and focal-adhesion systems optimizes rapid cell migration. Cell 125, 1361–1374.

Harrington AW, Ginty DD (2013). Long-distance retrograde neurotrophic factor signalling in neurons. Nat Rev Neurosci 14, 177–187.

Hengst U, Deglincerti A, Kim HJ, Jeon NL, Jaffrey SR (2009). Axonal elongation triggered by stimulus-induced local translation of a polarity complex protein. Nat Cell Biol 11, 1024–1030.

Huang EJ, Reichardt LF (2001). Neurotrophins: roles in neuronal development and function. Annu Rev Neurosci 24, 677–736.

Hur EM, Yang IH, Kim DH, Byun J, Saijilafu , Xu WL, Nicovich PR, Cheong R, Levchenko A, Thakor N, Zhou FQ (2011). Engineering neuronal growth cones to promote axon regeneration over inhibitory molecules. Proc Natl Acad Sci USA 108, 5057–5062.

Ichim G, Tauszig-Delamasure S, Mehlen P (2012). Neurotrophins and cell death. Exp Cell Res 318, 1221–1228.

Jurado C, Haserick JR, Lee J (2005). Slipping or gripping? Fluorescent speckle microscopy in fish keratocytes reveals two different mechanisms for generating a retrograde flow of actin. Mol Biol Cell 16, 507–518.

Ketschek AR, Jones SL, Gallo G (2007). Axon extension in the fast and slow lanes: substratum-dependent engagement of myosin II functions. Dev Neurobiol 67, 1305–1320.

Kollins KM, Hu J, Bridgman PC, Huang YQ, Gallo G (2009). Myosin-II negatively regulates minor process extension and the temporal development of neuronal polarity. Dev Neurobiol 69, 279–298.

Lee AC, Suter DM (2008). Quantitative analysis of microtubule dynamics during adhesion-mediated growth cone guidance. Dev Neurobiol 68, 1363–1377.

Letourneau PC (1975). Possible roles for cell-to-substratum adhesion in neuronal morphogenesis. Dev Biol 44, 77–91.

Lin CH, Espreafico EM, Mooseker MS, Forscher P (1996). Myosin drives retrograde F-actin flow in neuronal growth cones. Neuron 16, 769–782.

Lin CH, Forscher P (1995). Growth cone advance is inversely proportional to retrograde F-actin flow. Neuron 14, 763–771.

Liu RY, Schmid RS, Snider WD, Maness PF (2002). NGF enhances sensory axon growth induced by laminin but not by the L1 cell adhesion molecule. Mol Cell Neurosci 20, 2–12.

Loudon RP, Silver LD, Yee HF Jr, Gallo G (2006). RhoA-kinase and myosin II are required for the maintenance of growth cone polarity and guidance by nerve growth factor. J Neurobiol 66, 847–867.

Lowery LA, Van Vactor D (2009). The trip of the tip: understanding the growth cone machinery. Nat Rev Mol Cell Biol 10, 332–343.

Medeiros NA, Burnette DT, Forscher P (2006). Myosin II functions in actin-bundle turnover in neuronal growth cones. Nat Cell Biol 8, 215–226.

Mills J, Digicaylioglu M, Legg AT, Young CE, Young SS, Barr AM, Fletcher L, O'Connor TP, Dedhar S (2003). Role of integrin-linked kinase in nerve growth factor-stimulated neurite outgrowth. J Neurosci 23, 1638–1648.

Mitchison T, Kirschner M (1988). Cytoskeletal dynamics and nerve growth. Neuron 1, 761–772.

Mortimer D, Fothergill T, Pujic Z, Richards LJ, Goodhill GJ (2008). Growth cone chemotaxis. Trends Neurosci 31, 90–98.

Mortimer D, Pujic Z, Vaughan T, Thompson AW, Feldner J, Vetter I, Goodhill GJ (2010). Axon guidance by growth-rate modulation. Proc Natl Acad Sci USA 107, 5202–5207.

Ng J, Nardine T, Harms M, Tzu J, Goldstein A, Sun Y, Dietzl G, Dickson BJ, Luo L (2002). Rac GTPases control axon growth, guidance and branching. Nature 416, 442–447.

Oppenheim RW (1989). The neurotrophic theory and naturally occurring motoneuron death. Trends Neurosci 12, 252–255.

Pasapera AM, Schneider IC, Rericha E, Schlaepfer DD, Waterman CM (2010). Myosin II activity regulates vinculin recruitment to focal adhesions through FAK-mediated paxillin phosphorylation. J Cell Biol 188, 877–890.
Renaudin A, Lehmann M, Girault J, McKerracher L (1999). Organization of point contacts in neuronal growth cones. J Neurosci Res 55, 458–471.
Riedl J, Crevenna AH, Kessenbrock K, Yu JH, Neukirchen D, Bista M, Bradke F, Jenne D, Holak TA, Werb Z, *et al*. (2008). Lifeact: a versatile marker to visualize F-actin. Nat Methods 5, 605–607.
Robles E, Gomez TM (2006). Focal adhesion kinase signaling at sites of integrin-mediated adhesion controls axon pathfinding. Nat Neurosci 9, 1274–1283.
Rochlin MW, Itoh K, Adelstein RS, Bridgman PC (1995). Localization of myosin II A and B isoforms in cultured neurons. J Cell Sci 108, 3661–3670.
Rochlin MW, Wickline KM, Bridgman PC (1996). Microtubule stability decreases axon elongation but not axoplasm production. J Neurosci 16, 3236–3246.
Rodriguez OC, Schaefer AW, Mandato CA, Forscher P, Bement WM, Waterman-Storer CM (2003). Conserved microtubule-actin interactions in cell movement and morphogenesis. Nat Cell Biol 5, 599–609.
Schaefer AW, Kabir N, Forscher P (2002). Filopodia and actin arcs guide the assembly and transport of two populations of microtubules with unique dynamic parameters in neuronal growth cones. J Cell Biol 158, 139–152.
Schaefer AW, Schoonderwoert VT, Ji L, Mederios N, Danuser G, Forscher P (2008). Coordination of actin filament and microtubule dynamics during neurite outgrowth. Dev Cell 15, 146–162.
Stepanova T, Slemmer J, Hoogenraad CC, Lansbergen G, Dortland B, De Zeeuw CI, Grosveld F, van Cappellen G, Akhmanova A, Galjart N (2003). Visualization of microtubule growth in cultured neurons via the use of EB3-GFP (end-binding protein 3-green fluorescent protein). J Neurosci 23, 2655–2664.
Suter DM, Errante LD, Belotserkovsky V, Forscher P (1998). The Ig superfamily cell adhesion molecule, apCAM, mediates growth cone steering by substrate-cytoskeletal coupling. J Cell Biol 141, 227–240.
Suter DM, Schaefer AW, Forscher P (2004). Microtubule dynamics are necessary for SRC family kinase-dependent growth cone steering. Curr Biol 14, 1194–1199.
Tanaka EM, Kirschner MW (1991). Microtubule behavior in the growth cones of living neurons during axon elongation. J Cell Biol 115, 345–363.
Tucker BA, Rahimtula M, Mearow KM (2005). Integrin activation and neurotrophin signaling cooperate to enhance neurite outgrowth in sensory neurons. J Comp Neurol 486, 267–280.
Tucker BA, Rahimtula M, Mearow KM (2006). Laminin and growth factor receptor activation stimulates differential growth responses in subpopulations of adult DRG neurons. Eur J Neurosci 24, 676–690.
Tullio AN, Bridgman PC, Tresser NJ, Chan CC, Conti MA, Adelstein RS, Hara Y (2001). Structural abnormalities develop in the brain after ablation of the gene encoding nonmuscle myosin II-B heavy chain. J Comp Neurol 433, 62–74.
Turney SG, Bridgman PC (2005). Laminin stimulates and guides axonal outgrowth via growth cone myosin II activity. Nat Neurosci 8, 717–719.
Wen Z, Zheng JQ (2006). Directional guidance of nerve growth cones. Curr Opin Neurobiol 16, 52–58.
Yamashita T, Tucker KL, Barde YA (1999). Neurotrophin binding to the p75 receptor modulates Rho activity and axonal outgrowth. Neuron 24, 585–593.
Zhang XF, Schaefer AW, Burnette DT, Schoonderwoert VT, Forscher P (2003). Rho-dependent contractile responses in the neuronal growth cone are independent of classical peripheral retrograde actin flow. Neuron 40, 931–944.
Zhou FQ, Zhou J, Dedhar S, Wu YH, Snider WD (2004). NGF-induced axon growth is mediated by localized inactivation of GSK-3beta and functions of the microtubule plus end binding protein APC. Neuron 42, 897–912.